

# Understanding the Mechanism and Importance of Brown Carbon Bleaching Across the Visible Spectrum in Biomass Burning Plumes from the WE-CAN Campaign

Yingjie Shen<sup>1</sup>, Rudra P. Pokhrel<sup>1, a</sup>, Amy P. Sullivan<sup>2</sup>, Ezra J. T. Levin<sup>2, b</sup>, Lauren A. Garofalo<sup>3</sup>, Delphine K. Farmer<sup>3</sup>, Wade Permar<sup>4</sup>, Lu Hu<sup>4</sup>, Darin W. Toohey<sup>5</sup>, Teresa Campos<sup>6</sup>, Emily V. Fischer<sup>2</sup>, Shane M. Murphy<sup>1</sup>

<sup>1</sup>Department of Atmospheric Science, University of Wyoming, Laramie, WY 82071, USA.

<sup>2</sup>Department of Atmospheric Science, Colorado State University, Fort Collins, CO 80523, USA

<sup>3</sup>Department of Chemistry, Colorado State University, Fort Collins, CO 80523, USA

<sup>4</sup>Department of Chemistry and Biochemistry, University of Montana, Missoula, MT 59812, USA.

<sup>5</sup>Department of Atmospheric and Oceanic Sciences, University of Colorado Boulder, Boulder, CO 80309, USA

<sup>6</sup>National Center for Atmospheric Research, Atmospheric Chemistry Division, Boulder, CO 80301, USA

<sup>a</sup>now at Air Pollution Control Division, Colorado Department of Public Health and Environment, Denver, CO 80246, USA

<sup>b</sup>now at METEC Research Group, Colorado State University Energy Institute, Fort Collins, CO 80524, USA

Corresponding author: Shane M. Murphy (shane.murphy@uwoyo.edu)

**Abstract.** Aerosol absorption of visible light has an important impact on global radiative forcing. Wildfires are one of the major sources of light-absorbing aerosol, but there remains significant uncertainty about the magnitude, wavelength dependence, and bleaching of absorption from biomass burning aerosol. We collected and analyzed data from 21 Western United States wildfire smoke plumes during the 2018 WE-CAN airborne measurement campaign to determine the contribution of black carbon (BC), brown carbon (BrC), and lensing to the aerosol mass absorption cross-section (MAC). Comparison to commonly used parameterizations and modeling studies suggest model overestimation of absorption is likely due to incorrect BrC refractive indices. Modelers (Wang et al. 2018; Carter et al. 2021) invoke a bleaching process that decreases the MAC of organic aerosol (OA) to offset the overestimation of absorption in models. However, no evidence of decreasing MAC is observed in individual WE-CAN fire plumes or in aged plumes from multiple fires. A decrease in OA mass and water-soluble organic carbon (WSOC), both normalized by CO to correct for dilution, is observed with increasing oxygen to carbon (O:C) ratio and decreasing gas-phase toluene:benzene ratio, when data from all fires is combined and in half of individual fire plumes. This results in a strong decrease in total absorption at 405 nm and slight decrease at 660 nm with these chemical markers. These results demonstrate that changes in absorption with chemical markers of plume age are the result of decreasing OA rather than changes in the MAC of the organic material itself. While decreasing MAC or OA mass with aging could both be called bleaching, and can both correct overestimation of absorption in models, it's important to distinguish these two effects because decreasing OA mass will also decrease scattering, which will cause a significantly different net radiative effect. We also find that an average of 54% of non-BC absorption (23% total absorption) at 660 nm is from water-soluble BrC, confirming that BrC absorption is important across the visible spectrum. Quantification of significant BrC at red wavelengths and the observation of bleaching being caused by changes in OA with O:C and

Formatted: Superscript

Formatted: Space Before: 0 pt

37 toluene:benzene markers of plume age provide important improvements to our understanding of BrC and critical  
38 constraints on aerosol absorption in regional and global climate models.

## 39 1 Introduction

40 Atmospheric aerosol impact the climate system by directly scattering and absorbing solar radiation, by  
41 indirectly changing cloud properties, and through deposition that changes the surface albedo (McConnell et al., 2007;  
42 Sarangi et al., 2020). Biomass burning injects a large amount of primary organic aerosol (POA), secondary organic  
43 aerosol (SOA) and black carbon (BC) into the atmosphere every year. BC is somewhat poorly defined, but is generally  
44 considered to be insoluble, ~~and refractory, and have an absorption exponent near one, and includes a variety of~~Other  
45 materials such as ~~char, biochar, chareoal,~~ elemental carbon (EC), and soot (Wei et al., 2013) ~~are often very similar to~~  
46 ~~BC, but each is operationally defined by how it is measured.~~ Although it only represents a small fraction of aerosol  
47 mass, BC has a significant impact on the global energy budget due to its ability to strongly absorb solar radiation at  
48 all visible wavelengths. While still important, positive radiative forcing of BC is lower in IPCC AR6 (2022) than in  
49 IPCC AR5 (2013). Bond et al. (2013) estimated the direct radiative forcing for BC from 1750 to 2005 at the top of the  
50 atmosphere (TOA) to be  $+0.71 \text{ W m}^{-2}$ , with an uncertainty of 90% while the latest IPCC AR6 (2022) estimates effective  
51 radiative forcing for BC from 1750 to 2019 to be  $+0.11 (-0.2 \sim +0.42) \text{ W m}^{-2}$ . It is important to note that AR5 reported  
52 direct radiative forcing while AR6 reports effective radiative forcing. While BC is emitted from nearly all combustion  
53 processes, the largest global source of BC is thought to be biomass burning (Bond et al., 2013). Organic aerosol (OA)  
54 also absorbs visible light, but its absorption strongly depends on the wavelength of light (Kirchstetter and Novakov,  
55 2004). Non-BC light absorbing organic compounds are often called brown carbon (BrC) and they are usually co-  
56 emitted with BC or formed by secondary chemistry in biomass burning plumes (Andreae and Gelencsér, 2006). Unlike  
57 BC, which absorbs light from the UV to the IR, BrC absorption sharply increases in the UV and shorter visible portions  
58 of the spectrum and has been historically considered to be almost transparent near the red wavelengths (Andreae and  
59 Gelencsér, 2006; Bahadur et al., 2012; Liu et al., 2020). The global-mean TOA direct radiative forcing from BrC also  
60 shows a large uncertainty, with estimates ranging from  $+0.03 \text{ W m}^{-2}$  to  $+0.57 \text{ W m}^{-2}$  (Saleh, 2020). Wildfires in the  
61 Western U.S. have increased in recent decades (Westerling et al., 2006; Burke et al., 2021), and will continue  
62 increasing according to model predictions (Yue et al., 2013; Hurteau et al., 2014; Ford et al., 2018; Neumann et al.,  
63 2021). Therefore, quantitative studies of the radiative effects caused by BC and BrC emitted from wildfires are crucial  
64 for a better understanding of future climate and essential to improve climate models.

65 The large uncertainty in the radiative forcing from BC is caused both by uncertainties in emissions and by  
66 uncertainty in properties that affect its optics, such as size distribution, morphology, refractive index, and mixing state  
67 (Bond et al., 2006; Kleinman et al., 2020; Brown et al., 2021). For wildfires, most of the aerosol mass is organic  
68 (Garofalo et al., 2019). When BC is internally mixed with OA, the BC is coated by other absorbing or non-absorbing  
69 materials that cause more photons to interact with the BC core, and therefore enhance the absorption of the BC core.  
70 This process is often called the lensing effect even though geometric lensing is not actually happening at these sizes  
71 (Fuller et al., 1999). The absorption enhancement caused by the lensing effect is defined as the ratio of the absorption  
72 cross-section of a coated BC particle to that of an equivalent uncoated BC particle (Lack and Cappa, 2010). Laboratory

73 experiments have shown a strong absorption enhancement of BC by a factor of two or more (Schnaiter et al., 2003;  
74 Schnaiter et al., 2005; Bond and Bergstrom, 2006; Bond et al., 2006; Peng et al., 2016). Observations of absorption  
75 enhancement from ambient BC vary widely in field studies due to variations in coating thickness, coating material,  
76 source type, or methodological differences, but it is often much lower than laboratory values (Liu et al., 2015, 2017;  
77 Cappa et al., 2012, 2019; Healy et al., 2015; Krasowsky et al., 2016). Cappa et al. (2019) summarized absorption  
78 enhancements observed at the red end of the visible spectrum from 10 studies including ambient measurements, source  
79 sampling, and lab experiments. The absorption enhancement reported by those measurements ranged from 1.1 to 2.8.  
80 Lack et al. (2010) found that the absorption enhancement caused by the absorbing shell would be smaller than the  
81 absorption enhancement caused by the pure scattering shell. The non-spherical morphology of BC and the tendency  
82 of BC to compact when coated by organics also can both enhance and decrease absorption (Romshoo et al., 2021;  
83 Kelesidis et al., 2022).

84 The mass absorption cross section of BC ( $MAC_{BC}$ ) is ~~a different way~~ an alternative method to describe  
85 quantify the absorbing ability of BC containing particles versus absorption enhancement. By describing the absorption  
86 per unit mass of BC,  $MAC_{BC}$  can be a fundamental input in climate models to convert mass concentration into  
87 absorption coefficients (Cho et al., 2019).  $MAC_{BC}$  is the particulate absorption divided by the mass of the pure BC at  
88 the same a certain wavelength. In this way, the calculated  $MAC_{BC}$  will include absorption of the BC core along with  
89 the absorption and absorption enhancement caused by the coating material. Unfortunately, the MAC of the overall BC  
90 particle,  $MAC_{BC}$ , in the ambient atmosphere continues to be poorly understood due to a lack of field measurements  
91 and limitations of filter-based instruments to measure this parameter. Processes that occur during atmospheric aging  
92 of BC also introduce uncertainties in its absorption. Bond and Bergstrom (2006) suggested a  $MAC_{BC}$  of  $7.5 \pm 1.2 \text{ m}^2 \text{ g}^{-1}$   
93 <sup>1</sup> at 550 nm for fresh BC. The following campaigns demonstrate the variety of  $MAC_{BC}$  measured in the ambient during  
94 the past 15 years. Subramanian et al. (2010) reported a  $MAC_{BC}$  of  $10.9 \pm 2.1 \text{ m}^2 \text{ g}^{-1}$  at 660 nm and  $13.1 \text{ m}^2 \text{ g}^{-1}$  at 550  
95 nm over Mexico City when using a single particle soot photometer (SP2) and the filter-based particle soot absorption  
96 photometer (PSAP) instrument during airborne measurements. Krasowsky et al. (2016) reported a  $MAC_{BC}$   
97 enhancement of  $1.03 \pm 0.05$  due to the coatings on BC. Zhang et al. (2017) found a  $MAC_{BC}$  with a mean of  $10 \text{ m}^2 \text{ g}^{-1}$   
98 and a standard deviation of  $4 \text{ m}^2 \text{ g}^{-1}$  at 660 nm by using both SP2 and PSAP measurements. Cho et al. (2019)  
99 summarized  $MAC_{BC}$  estimated from more than 10 studies in East and South Asia in both ambient conditions and  
100 laboratory experiments, and the values ranged from 4.6 to  $11.3 \text{ m}^2 \text{ g}^{-1}$ .

101 The limitations of current measurement techniques bring major uncertainty into quantifying BrC absorption,  
102 because BrC is usually co-emitted with BC which makes it challenging to measure BrC absorption independently.  
103 BrC absorption can be directly measured through the solvent-extraction method (Peltier et al., 2007; Zeng et al., 2021;  
104 Sullivan et al., 2022) or a thermodenuder (Cappa et al., 2012; Liu et al., 2015; Pokhrel et al., 2017). However, the  
105 solvent-extraction method will miss BrC that's insoluble in water or organic solvents, and thermal denuders miss BrC  
106 that is not volatile at the denuder temperature. BrC absorption can also be calculated from multi-wavelength total  
107 absorption measurements, but this approach must assume the absorption Ångström exponent (AAE) for BC and  
108 assumes that BrC does not absorb at longer wavelengths, adding significant uncertainty.

Formatted: Subscript

109 To improve understanding of the evolution of light-absorbing aerosol from biomass burning, smoke from 21  
110 wildfires in the Western United States were measured near their sources and downwind onboard the NSF/NCAR C-  
111 130 aircraft during the Western Wildfire Experiment for Cloud Chemistry, Aerosol Absorption and Nitrogen (WE-  
112 CAN) campaign. This campaign represented an airborne attempt to fully characterize Western U.S. wildfires from  
113 several different fuel types, locations, and fire stages (flaming vs. smoldering). This paper presents novel observations  
114 about the absorbing properties of the aerosol and compares these observations to modeling studies conducted with the  
115 WE-CAN data and to results from the Fire Influence on Regional to Global Environment – Air Quality (FIREX) study  
116 conducted in 2019 (Zeng et al., 2021).

## 117 **2 Experimental Method**

118 This work relies on measurements made during the WE-CAN field campaign, which sampled smoke emitted  
119 by wildfires across the Western U.S. using the NSF/NCAR C-130 research aircraft. The goal of the campaign was to  
120 make detailed observations of the physical, chemical, and optical evolution of aerosol in western wildfire smoke and  
121 its impact on climate, air quality, weather, and nutrient cycles. The WE-CAN field campaign consisted of 19 research  
122 flights that took place from Jul. 24 – Sep. 13, 2018. Data from 13 flights where all required instrumentation was  
123 available were analyzed in this study. The flight path and dominant wildfire for each of these flights are shown in Fig.  
124 1. The fire locations, fuel types for each fire during WE-CAN were characterized and summarized by Lindaas et al.  
125 (2021).

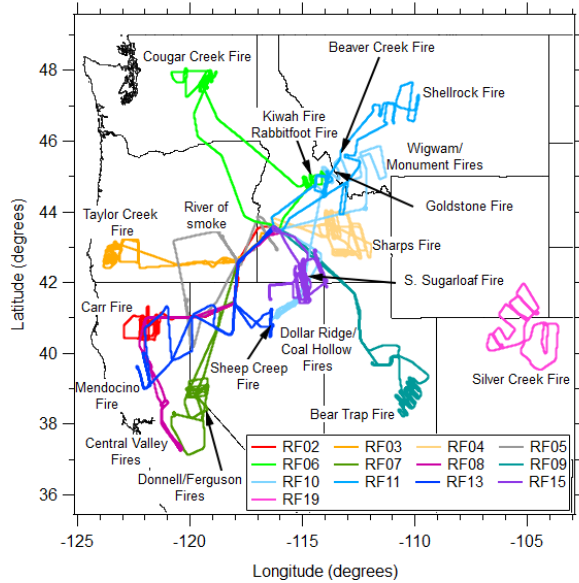


Figure 1: Flight paths and the sampled wildfires for the WE-CAN flights analyzed in this paper.

126 **2.1 Instrumentation**

127 The following instruments are a subset of those flown during the WE-CAN campaign and are utilized in this  
 128 work. The full WE-CAN dataset is archived at [https://data.eol.ucar.edu/master\\_lists/generated/we-can](https://data.eol.ucar.edu/master_lists/generated/we-can). All aerosol  
 129 instruments utilized in this paper, except the PILS, pulled air from the same Solid Diffuser Inlet (SDI) inlet. The PILS  
 130 sampled from a Submicron Aerosol Inlet (SMAI) (Craig et al., 2013a, 2013b, 2014; Moharreri et al., 2014). All the  
 131 measurements were converted to standard temperature and pressure (STP, 1 atm, 0°C) based on the measured  
 132 temperature and pressure (Eq. 1) before data were uploaded (Palm et al., 2020; Sullivan et al., 2022).

133 
$$Variables_{STP} = Variables_{measured} \cdot \frac{Pressure_{STP}}{Pressure_{measured}} \cdot \frac{Temperature_{measured}}{Temperature_{STP}} \quad (Eq. 1)$$

134 **2.1.1 Photoacoustic Absorption Spectrometer (PAS)**

135 Aerosol absorption coefficients were measured with the multi-wavelength PAS built by the University of  
 136 Wyoming (Foster et al., 2019), based on the design of Lack et al. (2012b). A PAS can directly measure the absorption  
 137 coefficient of dry aerosol. The PAS represents the only way to directly measure aerosol absorption other than a  
 138 photothermal interferometer (PTI, Sedlacek, 2007), which measures the change in the refractive index of the air near  
 139 particles caused by heating from absorption. Briefly, when modulated laser light (at the resonant frequency of the cell)  
 140 is absorbed by the aerosol it heats the surrounding air inducing pressure waves that are amplified by the cavity then  
 141 detected by two microphones (Lack et al., 2006; Foster et al., 2019). The PAS used here has four cells that measure

142 the aerosol absorption coefficient from dry air at 405 nm and 660 nm and thermally denuded air at 405 nm and 660  
143 nm. The denuder was set to 300°C, with the goal of evaporating volatile organic aerosol which might have a potential  
144 impact on light absorption. However, absorption from the denuded channels was not used in this study, because the  
145 absorption enhancement calculated using the thermodenuder approach was much smaller than the approach taking the  
146 ratio of  $MAC_{BC}$  to  $MAC_{BC-core}$ , and we believe the discrepancy is due to the presence of significant residual organic  
147 material after denuding. Two  $NO_X$  denuders coated with potassium hydroxide, guaiacol and methanol were installed  
148 on the PAS in front of the inlet to remove the absorption from gas-phase  $NO_2$  (Williams and Grosjean 1990). No  
149 evidence of  $NO_2$  absorption (which would cause baseline shifts) was observed during filter measurements that are  
150 acquired every few minutes. A 3 LPM  $PM_{2.5}$  cyclone (URG-2000-30ED) was used on the PAS in front of the inlet to  
151 provide a  $PM_{1.0}$  cut under a total flow rate of 5.7 LPM. In addition, a Nafion drier (Purma Pure PD-100T-24MPS)  
152 with 100 tubes was installed on the inlet system to dry sample to a relative humidity below 30%. The particle loss (<  
153 3%) in the drier was corrected during post-processing. The uncertainty in the absorption coefficient measured by the  
154 PAS mainly comes from the calibration technique, in which the highly absorbing substance Regal Black and the CAPS  
155  $PM_{SSA}$  were utilized (Foster et al., 2019). The PAS was routinely calibrated (after each flight or every other day if  
156 there was a flight everyday) during WE-CAN with an accuracy of +/- 10%.

157 The PAS microphone shows a pressure-dependent response to pressure. To account for this behavior, we  
158 performed pressure-dependent calibration of the PAS where the instrument pressure (both PAS and CAPS  $PM_{SSA}$ )  
159 was dropped stepwise by ~50 torr from ambient to ~300 torr (typical minimum pressure level during WE-CAN). A  
160 calibration was performed at each pressure step and the calibration constants were fitted with pressure to get a change  
161 in calibration at a desired pressure. Pressure-dependent calibrations were repeated pre and post-campaign to capture  
162 variability.

### 163 2.1.2 Cavity-Attenuated Phase Shift Spectrometer (CAPS $PM_{SSA}$ )

164 After pulling through the  $NO_X$  denuder, the  $PM_{1.0}$  cyclone, and the Nafion drier in front of the PAS inlet, the  
165 sampled air entered through the Aerodyne CAPS  $PM_{SSA\_450}$  and CAPS  $PM_{SSA\_660}$  to measure the aerosol scattering  
166 and extinction coefficients at 450 nm and 660 nm, respectively. CAPS  $PM_{SSA}$  instruments measure extinction by  
167 utilizing the cavity attenuated phase shift spectroscopy and measure scattering with an integrating sphere (Onasch et  
168 al., 2015). Ammonium sulfate particles were used to calibrate the scattering channel of the CAPS  $PM_{SSA}$  during WE-  
169 CAN with an accuracy of +/- 3%.

### 170 2.1.3 Particle-into-Liquid Sampler (PILS) systems

171 BrC absorption and water-soluble organic carbon (WSOC) were measured by a Particle-into-Liquid Sampler  
172 (PILS) system (Sullivan et al., 2022). The PILS continuously collects ambient particles into purified water and  
173 provides a liquid sample with the aerosol particles dissolved in it for analysis (Orsini et al., 2003). The size-cut for the  
174 PILS was provided by a nonrotating microorifice uniform deposit impactor (MOUDI) with a 50% transmission  
175 efficiency of 1  $\mu m$  (aerodynamic diameter) at 1 atmosphere ambient pressure (Marple et al., 1991). The total airflow  
176 for the PILS was approximately 15 LPM. Upstream of the PILS was an activated carbon parallel plate denuder

177 (Eatough et al., 1993) to remove organic gases. In addition, a valve was manually closed periodically for 10 min  
178 diverting the airflow through a Teflon filter before entering the PILS allowing for background measurements. The  
179 liquid sample obtained from the PILS was pushed through a 0.2  $\mu\text{m}$  PTFE liquid filter by a set of syringe pumps to  
180 ensure insoluble particles were removed. The flow was then directed through a liquid waveguide capillary cell (LWCC)  
181 and Total Organic Carbon (TOC) Analyzer for near real-time measurement of BrC absorption and WSOC,  
182 respectively. More details and a schematic illustration can be found in Zeng et al. (2021).

183 For the absorption measurement, a 2.5 m path-length LWCC (World Precision Instruments, Sarasota, FL)  
184 was used. A dual deuterium and tungsten halogen light source (DH-mini, Ocean Optics, Largo, FL) and absorption  
185 spectrometer (FLAME-T-UV-VIS, Ocean Optics, Largo, FL) were coupled to the LWCC via fiber optic cables.  
186 Absorption spectra were recorded using the Oceanview Spectroscopy Software over a range from 200 to 800 nm. The  
187 wavelength-dependent absorption was calculated following the method outlined in Hecobian et al. (2010). For this  
188 study, a 16 s integrated measurement of absorption with a limit of detection (LOD) of 0.1  $\text{Mm}^{-1}$  was obtained (Sullivan  
189 et al., 2022).

190 For the WSOC measurement, a Sievers Model M9 Portable TOC Analyzer (Suez Waters Analytical  
191 Instruments, Boulder, CO) was used. This analyzer works by converting the organic carbon in the liquid sample to  
192 carbon dioxide through chemical oxidation involving ammonium persulfate and ultraviolet light. The carbon dioxide  
193 formed was then measured by conductivity. The increase in conductivity observed was proportional to the amount of  
194 organic carbon in the liquid sample. The analyzer was run in turbo mode providing a 4 s integrated measurement of  
195 WSOC with a LOD of 0.1  $\mu\text{g C/m}^3$  (Sullivan et al., 2022).

#### 196 **2.1.4 Single Particle Soot Photometer (SP2)**

197 Refractory black carbon (rBC) number and mass concentrations were measured with a Single Particle Soot  
198 Photometer (SP2; Droplet Measurement Technologies) which uses a continuous, 1064 nm Nd:YAG laser to heat  
199 absorbing material, primarily rBC, to its vaporization temperature and measures the resulting incandescence (Schwarz  
200 et al., 2006). Similar to the CAPS  $\text{PM}_{\text{SSA}}$ , the sampled air was sent through the  $\text{NO}_x$  denuder,  $\text{PM}_{1.0}$  cyclone, and  
201 Nafion drier in front of the PAS inlet before it went to the SP2. The SP2 was calibrated with PSL and size-selected  
202 fullerene soot. On the C-130, the SP2 sample line was diluted with HEPA-filtered, pressured ambient air that was  
203 passed through a mass flow controller to prevent signal saturation. During post-processing the data was corrected for  
204 dilution back to ambient concentrations.

#### 205 **2.1.5 Ultra-High Sensitivity Aerosol Spectrometer (UHSAS)**

206 Particle number concentration was measured by a rack-mounted Ultra-High Sensitivity Aerosol Spectrometer  
207 (UHSAS). The flow rate of the rack-mounted UHSAS can be manually lowered by the in-flight operator when the  
208 aircraft flew across smoke plumes, so that the UHSAS can stay within its optimum concentration measurement range  
209 (Sullivan et al., 2022). The UHSAS was calibrated with ammonium sulfate. The particle mass concentration was  
210 calculated by applying these size bins and multiplying by a particle density of 1.4  $\text{g cm}^{-3}$  (Sullivan et al., 2022). The  
211 volume mean diameter of the particles for all the detected plumes range between 0.18  $\mu\text{m}$  and 0.34  $\mu\text{m}$ .

212 **2.1.6 Proton-Transfer-Reaction Time-of-Flight Mass Spectrometer (PTR-ToF-MS)**

213 The University of Montana proton-transfer-reaction time-of-flight mass spectrometer (PTR-ToF-MS 4000,  
214 Ionicon Analytik) was utilized to report the VOC mixing ratios during WE-CAN (Permar et al., 2021). Only the  
215 toluene and benzene mixing ratio derived from the PTR-ToF-MS were used in this work; their overall uncertainty is  
216 < 15%. More details of the operation, calibration, and validation on the PTR-ToF-MS during WE-CAN can be found  
217 in Permar et al. (2021).

218 **2.1.7 High-Resolution Aerosol Mass Spectrometry (HR-AMS)**

219 Organic aerosol (OA) was detected by the high-resolution aerosol mass spectrometry (HR-AMS; Aerodyne  
220 Inc.). The description of the AMS operation during WE-CAN can be found in Garofalo et al. (2019). The atomic  
221 oxygen-to-carbon ratios (O:C) and organic mass-to-organic carbon ratio (OM:OC) used in this work were determined  
222 via the improved ambient elemental analysis method for the AMS (Canagaratna et al., 2015). Average (integrated)  
223 elemental ratios were obtained by averaging (integrating) elemental masses of carbon, hydrogen, and oxygen and  
224 recalculating elemental ratios.

225 **2.1.8 Quantum Cascade Laser (QCL) and Picarro Cavity Ring-Down spectrometer (Picarro)**

226 The carbon monoxide (CO) mixing ratio was measured by both an Aerodyne quantum cascade laser  
227 instrument (CS-108 miniQCL) and a Picarro cavity ring-down spectrometer (G2401-m WS-CRD) (Garofalo et al.,  
228 2019). Because the QCL has better precision than the Picarro instrument, CO measurements from the QCL were  
229 preferentially used. However, CO measurements from the Picarro CO data were used for RF10 and RF13, because the  
230 CO-QCL was not operated during those two flights. The carbon dioxide (CO<sub>2</sub>) mixing ratio was also determined from  
231 the Picarro.

232 **2.2 Plume Physical Age**

233 The physical age of the plume was calculated by dividing the distance the plume was sampled from the fire  
234 source by the in-plume average wind speed. The average wind speed was measured on the NSF/NCAR C-130 aircraft  
235 during each plume pass. The distance was estimated by using the longitude and latitude of the geometric center of the  
236 plume measured on the NSF/NCAR C-130 and the fire location provided by the U.S. Forest Service. The same method  
237 was used by Garofalo et al. (2019), Peng et al. (2020), Lindaas et al. (2021), Permar et al. (2021), and Sullivan et al.  
238 (2022) and are also utilized here for consistency.

239 **2.3 Plume Integration Method**

240 During the WE-CAN campaign, both the SP2 and PILS had significant hysteresis compared to other  
241 instruments. In the SP2 this is because the sampled air was diluted with particle-free ambient air at various ratios to  
242 prevent signal saturation. In the PILS this is because of the retention effect of liquid on the wetted component or within  
243 dead volumes (Zeng et al., 2021). Therefore, it was most accurate to integrate properties across airborne transects of  
244 wildfire plumes to avoid the impact of instrument hysteresis and measurement noise that can dramatically impact



245 instantaneous ratios. Pseudo-Lagrangian sampling was used during the flights for the WE-CAN campaign, the C-130  
 246 aircraft repeatedly crossed the smoke plume from a particular fire by traveling perpendicular to the prevailing winds,  
 247 crossing the plume, turning, then crossing the plume again further downwind. In this work, we manually identified  
 248 plume edges based on the inflection point when CO concentrations stopped rapidly changing as we entered and exited  
 249 the smoke plume. The outside of plume measurement periods had CO mixing ratios from 100 - 300 ppbv. The lowest  
 250 10% of each variable from outside plume segments were set to be the background of that variable. If the time between  
 251 two consecutive outside plume segments was larger than 20 s and the highest CO mixing ratio was 100 ppbv higher  
 252 than the outside plume CO criteria, this segment was chosen as a plume. The start and end point of each plume was  
 253 slightly adjusted manually based on the CO mixing ratio to make sure the entire plume was covered. A different start  
 254 and end point for the SP2 and PILS was adjusted manually based on the rBC mass concentrations and WSOC,  
 255 respectively.

#### 256 2.4 Absorption Enhancement and Mass Absorption Cross-section

257 Absorption enhancement ( $E_{abs}$ ) is the ratio of the absorption of all particles (including BC core and coating  
 258 materials) to the absorption of BC alone (Lack and Cappa, 2010).  $E_{abs}$  at a specific wavelength 660 nm ( $E_{abs, \lambda 660}$ )  
 259 was calculated in this study by Eq. 2:

$$E_{abs, \lambda 660} = \frac{Abs_{Total, \lambda 660}}{M_{BC} * MAC_{BC, core, \lambda 660}} \quad (Eq. 2)$$

260 where  $Abs_{Total, \lambda 660}$  is the total absorption coefficient at a wavelength of 660 nm measured by the PAS,  $M_{BC}$  is the  
 261 mass concentration of BC measured by the SP2, and  $MAC_{BC, core, \lambda 660}$  is the MAC of BC alone (without any other  
 262 coating material) at 660 nm, which is set to be  $6.3 \text{ m}^2 \text{ g}^{-1}$  at 660 nm (Bond and Bergstrom, 2006; Subramanian et al.,  
 263 2010).

265  $MAC_{BC}$  at 660 nm was calculated following Eq. 3:

$$MAC_{BC, \lambda 660} = \frac{Abs_{Total, \lambda 660}}{M_{BC}} \quad (Eq. 3)$$

267  $MAC_{BC, \lambda 660}$  is utilized more often in this study than  $E_{abs, 660}$  because there is not a widely accepted MAC  
 268 for BC emitted from wildfire. MAC of BrC and lensing is calculated at 405 and 660 nm (Eq. 4):

$$MAC_{BrC+lensing, \lambda} = \frac{Abs_{Total, \lambda} - M_{BC} * MAC_{BC, core, \lambda}}{M_{OA}} \quad (Eq. 4)$$

270 where  $M_{OA}$  is the organic mass measured by the AMS. Again, the  $MAC_{BC, core, \lambda}$  is set to be  $6.3$  and  $10.2 \text{ m}^2 \text{ g}^{-1}$ ,  
 271 respectively, at 660 nm and 405 nm yielding an absorption Ångström exponent (AAE, the negative slope of a  
 272 logarithmic absorption coefficient against wavelength) of 0.99 for the BC core (Bond and Bergstrom, 2006;  
 273 Subramanian et al., 2010; Liu, et al., 2015). It should be noted that both BrC and lensing contribute to the  
 274  $MAC_{BrC+lensing, \lambda}$ , and cannot be separated using this approach and:  $MAC_{BrC+lensing, \lambda}$  is the MAC of all organics without  
 275 distinguishing absorbing and non-absorbing particles.

276 MAC of water-soluble BrC at  $\lambda$  nm ( $MAC_{ws, BrC, \lambda}$ ) is calculated using Eq. 5:

$$MAC_{ws, BrC, \lambda} = \frac{Abs_{ws, BrC, \lambda}}{WSOC * (WSOM:WSOC)} \quad (Eq. 5)$$

Formatted: Indent: First line: 0.5"

Formatted: Font: Symbol

Formatted: Font: 10 pt

278 where  $Abs_{ws\_BrC\_660}$  is water-soluble light absorption and WSOC is water-soluble organic carbon mass, which are  
 279 both measured by the PILS system. WSOM:WSOC ratio is set to be 1.6 (Sullivan et al., 2022). MAC<sub>ws\_BrC</sub> is the  
 280 MAC of all water-soluble organics without distinguishing absorbing and non-absorbing particles.

## 281 2.5 Fractional non-BC Absorption from BrC

282 Many previous studies of BrC assume that BrC does not absorb significant amounts of light at long  
 283 wavelengths (532~705 nm) (Wonaschütz et al., 2009; Lack et al., 2012a; Taylor et al., 2020; Zeng et al., 2021, Zhang  
 284 et al., 2022). In this study, a PILS system was used to quantify the absorption of light for water-soluble BrC at 660  
 285 nm. This absorption is not likely caused by traditional BC, which is insoluble and will be removed by the PILS  
 286 impactor, the 0.2 µm filter in the PILS, and that BC over 110 nm in size will not be oxidized by the TOC analyzer  
 287 (Peltier et al., 2007; Zeng et al., 2021; Sullivan et al., 2022).

288 To investigate which contributes more to absorption enhancement at 660 nm, the absorption from BrC or  
 289 the lensing effect, the fractional non-BC absorption from BrC at 660 nm is calculated by Eq. 6

$$290 \text{ Fractional } Abs_{BrC} = \frac{Abs_{BrC\_660}}{Abs_{Total\_660} - M_{BC} * MAC_{BC\_core\_660}} \quad (Eq. 6)$$

291 where  $Abs_{Total\_660}$  is the total absorption coefficient at 660 nm which is measured by the PAS,  $M_{BC}$  is the mass  
 292 concentration of BC which is measured by the SP2, and  $MAC_{BC\_core\_660}$  is the MAC of the BC core at 660 nm which  
 293 is set to be 6.3 m<sup>2</sup> g<sup>-1</sup> (Bond and Bergstrom, 2006; Subramanian et al., 2010).  $Abs_{BrC\_660}$  is the total BrC absorption  
 294 coefficient at 660 nm, which is calculated from the water-soluble light absorption provided by the PILS, where we  
 295 convert absorption from water-soluble BrC to total BrC. More specifically, to convert the measured light absorption  
 296 by water-soluble organics into total BrC absorption in the ambient, it had to be multiplied by two factors. The first  
 297 factor converts absorption from water-soluble BrC into absorption from total BrC. This factor is obtained by taking  
 298 the ratio between total particulate organic mass and water-soluble particulate organic mass (OM:WSOM). Water-  
 299 soluble organic mass is calculated from the PILS WSOC data using a WSOM:WSOC (water-soluble organic mass :  
 300 water-soluble organic carbon) ratio of 1.6 (Duarte et al., 2015 & 2019). Ambient organic mass is measured by the  
 301 AMS or calculated from the particle size distributions measured by the UHSAS assuming the particle mass all comes  
 302 from organic material with a particle density of 1.4 g cm<sup>-3</sup>. Both methods are used and compared in this paper. The  
 303 second factor accounts for the fact that particles absorb more light than the same substance in the bulk liquid phase.  
 304 Here we use Mie theory (Bohren and Huffman, 1983) to convert absorption from BrC in aqueous solution to the  
 305 absorption from BrC particles in the ambient (Liu et al., 2013; Zeng et al., 2020). The complex refractive index ( $m =$   
 306  $n + ik$ ) was put into a Mie code (implemented into Igor by Ernie R. Lewis base on Bohren and Huffman, 1983) to  
 307 obtain the absorption efficiency ( $Q$ ), and further used to calculate the absorption coefficient by Eq. 7 (Liu et al., 2013).  
 308 The real part of the refractive index ( $n$ ) is set to be 1.55, and the imaginary part is calculated by using Eq. 8 (Liu et al.,  
 309 2013).

$$310 Abs(\lambda, D_p) = \frac{3}{2} \cdot \frac{Q \cdot WSOC}{D_p \cdot \rho} \quad (Eq. 7)$$

$$311 k = \frac{\rho \lambda \cdot H_2O\_Abs(\lambda)}{4\pi \cdot WSOC} \quad (Eq. 8)$$

312 where  $\lambda$  is the wavelength,  $D_p$  is the diameter of the particle,  $Abs(\lambda, D_p)$  is absorption coefficient,  $Q$  is absorption  
 313 efficiency, particle density ( $\rho$ ) is set to be  $1.4 \text{ g cm}^{-3}$ ,  $WSOC$  is the mass concentration of WSOC ( $\mu\text{gC m}^{-3}$ ) measured  
 314 by the PILS, and  $H_2O\_Abs(\lambda)$  is the water-soluble light absorption coefficient measured by PILS. The plume averaged  
 315 particle size distribution was used in the calculation, then the absorption coefficient was calculated for each size bin  
 316 of UHSAS to obtain the most accurate Mie factor for each plume.

317 The average OM:WSOM factor based on the UHSAS (UHSAS factor) for all the plumes is 2.36 with a  
 318 standard deviation is 1.17. The averaged OM:WSOM based on the AMS (AMS factor) is 1.63 with a standard  
 319 deviation of 0.74. The average Mie factor at 660 nm is 1.47 (standard deviation of 0.13), which is close to the factor  
 320 of 1.36 found by Zeng et al. (2022) based on FIREX data. The Mie factor at 405 nm based on the WE-CAN data is  
 321 also calculated, with an average of 1.83, which is similar to the factor that Zeng et al. (2022) determined at 405 nm  
 322 (1.7) based on FIREX and Liu et al. (2013) determined at 450 nm (1.9) based on measurements in Atlanta.

323 Sensitivity tests were done on these factors by choosing reasonable ranges of particle density ( $1.1 \text{ g cm}^{-3}$ ,  $1.4$   
 324  $\text{g cm}^{-3}$  and  $1.7 \text{ g cm}^{-3}$ ) and WSOM:WSOC ratio (1.5, 1.6 and 1.8) (Duarte et al., 2015 & 2019; Finessi, et al., 2012;  
 325 Sun et al., 2011) (Table S1). Particle density only affects the Mie factor and UHSAS factor, while WSOM:WSOC  
 326 ratio affects the AMS factor and UHSAS factor. As shown in Table S1, the impact of particle density on the Mie factor  
 327 (both at 660 nm and 405 nm) is negligible, WSOM:WSOC is the only component that affects the AMS factor (ranging  
 328 from 1.48 to 1.73), while the UHSAS factor is much more sensitive (ranging from 1.65 to 3.06) to both particle density  
 329 and WSOM:WSOC. Overall, Table S1 demonstrates that none of the factors other than the UHSAS factor are sensitive  
 330 to the exact parameters chosen for the calculation, giving confidence that the results presented are robust.

331 This approach assumes that water insoluble BrC has the same refractive index as water soluble BrC. This  
 332 assumption would provide a lower estimation on the BrC contribution to the total absorption because Sullivan et al.  
 333 (2022) found that 45% of the BrC absorption at 405 nm in WE-CAN came from water-soluble species, and Zeng et  
 334 al. (2022) found that insoluble BrC absorbs more at higher wavelengths than soluble BrC, and methanol-insoluble  
 335 BrC chromophores caused 87% of the light absorption at 664 nm.

## 336 2.6 Absorption of BrC and Water-soluble BrC

337 The bulk absorption coefficient of water-soluble BrC at a specific wavelength ( $Abs_{ws\_BrC\lambda}$ ) is measured by  
 338 PILS system directly. The bulk absorption coefficient of BrC is calculated from Eq. 9:

$$339 \quad Abs_{BrC+lensing,\lambda} = Abs_{Total,\lambda} - M_{BC} * MAC_{BCcore,\lambda} \quad (Eq. 9)$$

340 where the  $Abs_{Total,\lambda}$  is the total absorption coefficient measured by the PAS. MAC of the BC core is set to  
 341 be  $6.3$  and  $10.2 \text{ m}^2 \text{ g}^{-1}$ , respectively, at 660 nm and 405 nm. It should be noted that both BrC and lensing contribute to  
 342 the bulk absorption coefficient, and cannot be separated using this approach.

343 Then the plume integrated absorption and scattering were normalized ( $x/CO$ ) by taking the ratio of  
 344 background-subtracted absorption or scattering ( $\Delta x$ ) to the background-subtracted  $CO$  mixing ratio ( $\Delta CO$ ) (Eq. 10),  
 345 so that the changing of the normalized properties is not impacted by dilution of the plume with background air.

$$346 \quad x/CO = \frac{\Delta x}{\Delta CO} \quad (Eq. 10)$$

## 347 2.7 Modified Combustion Efficiency (MCE)

348 The variation of burn condition (e.g., flaming vs. smoldering) and fuel type can cause a significant difference  
349 in BC emissions and changes in aerosol properties (Akagi et al., 2011; Andreae, 2019). Burn conditions can be  
350 estimated with the modified combustion efficiency (MCE), defined as Eq. 11:

$$351 \text{MCE} = \frac{\Delta\text{CO}_2}{\Delta\text{CO} + \Delta\text{CO}_2} \quad (\text{Eq. 11})$$

352 where  $\Delta\text{CO}_2$  and  $\Delta\text{CO}$  are the background-subtracted  $\text{CO}_2$  and  $\text{CO}$  mixing ratio. The background of  $\text{CO}_2$  and  $\text{CO}$   
353 mixing ratio is obtained via the same process described in Section 2.3.

## 354 3 Results and Discussion

### 355 3.1 Comparison of WE-CAN $\text{MAC}_{\text{BrC}}$ to Modeling Studies

356 It is challenging for climate models to simulate absorption from BrC, especially because it is highly  
357 wavelength dependent and may change with chemical age (Liu et al., 2020). Recently the Saleh et al. (2014)  
358 parameterization has been implemented in models in an attempt to better parameterize the imaginary part of the BrC  
359 refractive index (Wang et al., 2018; Carter et al., 2021). To test how accurately the Saleh parameterization matched  
360 WE-CAN data, the BC:OA ratios measured during WE-CAN were input into the Saleh parameterization, which  
361 provides an imaginary part for the refractive index of BrC ( $k_{\text{BrC},\lambda}$ ) as a function of the BC:OA ratio. The plume  
362 integrated BC:OA ratio for each plume was used in the parameterization, which gave an average  $k_{\text{BrC}}$  of 0.025, 0.013,  
363 0.009, respectively, at 405 nm, 550 nm and 660nm. Mie theory (Bohren and Huffman, 1983) was then used to calculate  
364 the MAC for BrC. To do the Mie calculations we assumed a real part of the refractive index of 1.7 for BrC (same as  
365 Saleh et al., 2014), used volume mean diameters measured for each plume, and used an organic density of  $1.4 \text{ g cm}^{-3}$ .  
366 Figure 2 compares the observed  $\text{MAC}_{\text{BrC+lensing}}$  (Eq. 4) and  $\text{MAC}_{\text{ws\_BrC}}$  (Eq. 5) with the value calculated from the Saleh  
367 parameterization with inputs from WE-CAN. In both the observations and the parameterization, the  $\text{MAC}_{\text{BrC}}$  decreases  
368 as wavelength increases. However, the Saleh parameterization is always significantly larger than the observations.  
369 The  $\text{MAC}_{\text{BrC}}$  from the Saleh parameterization, which does not include lensing effects, is a factor of 3.4 and 2.8 larger  
370 than the observed  $\text{MAC}_{\text{BrC+lensing}}$  at 405 nm and 660 nm, respectively. The range of BC:OA ratios during WE-CAN  
371 (0.007~0.061) is on the very small end of the range (0.005~0.7) used in Saleh's work, and the parameterization failed  
372 to capture absorbing aerosol properties for this study. The discrepancy could also be partly because the data Saleh et  
373 al. used for their parameterization comes from controlled laboratory burns and not wildfires or because emissions  
374 observed during WE-CAN have all undergone some near-source aging before being observed by the aircraft. It is  
375 worth noting that the Saleh parameterization of  $\text{MAC}_{\text{BrC}}$  is very sensitive to organic aerosol density. If particle density  
376 is increased from  $1.4 \text{ g cm}^{-3}$  to  $1.7 \text{ g cm}^{-3}$ , the Saleh parameterization median  $\text{MAC}_{\text{BrC}}$  decreases to  $1.6 \text{ m}^2 \text{ g}^{-1}$  and  $0.24$   
377  $\text{m}^2 \text{ g}^{-1}$ , respectively, at 405 nm and 660 nm (a factor of 2.8 and 2.3, respectively, compared to observed  $\text{MAC}_{\text{BrC}}$  at  
378 405 nm and 660 nm). The fact that the Saleh parameterization overestimates the absorption property of biomass aerosol  
379 especially for fresh emitted aerosols suggests that different parameterizations are needed for the Western U.S.. Carter  
380 et al. (2021) utilized the Saleh parameterization for BrC absorption in the GEOS-Chem model and also found that the

381 Saleh model overestimated BrC absorption for WE-CAN. It was hypothesized that the overestimation was due to the  
 382 lack of a bleaching process for BrC in the model and offset part of the overestimation by bringing in bleaching into  
 383 the model.

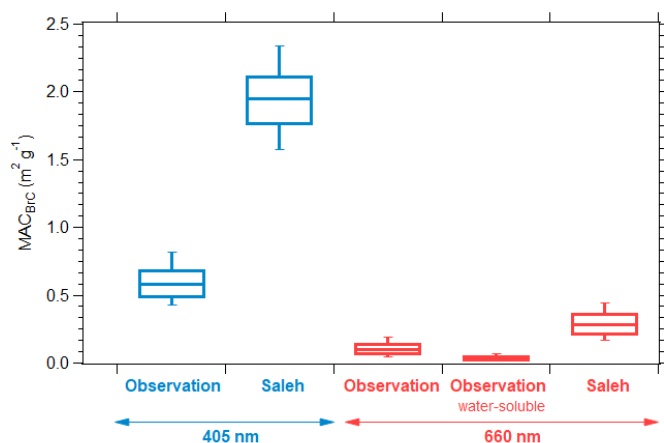


Figure 2: Boxplot summary for observed and parameterized (Saleh) MAC<sub>BrC</sub> at 405 nm (blue) and 660 nm (red). For each box, the central line represents the median, the top and bottom edges represent the 75<sup>th</sup> and 25<sup>th</sup> percentile, and the top and bottom whiskers represent the 90<sup>th</sup> and 10<sup>th</sup> percentile of the data.

### 384 3.2 Investigation of BrC Bleaching at Visible Wavelengths

385 A limited number of field measurements have shown BrC decay with chemical age (Forrister et al., 2015;  
 386 Wang et al., 2016). Despite a relatively poor understanding of the mechanism of bleaching or whitening of BrC, this  
 387 process has been implemented in numerous model simulations (Brown et al., 2018; Wang et al., 2018; Carter et al.,  
 388 2021). While only a fraction of organic aerosol mass absorbs light, both models and observations typically treat all  
 389 organics as equally absorbing because of the inability to distinguish absorbing and non-absorbing molecules. The  
 390 definition of bleaching or whitening is was unclear in previous literature, models Models tend to treat bleaching as  
 391 the change of refractive index or decreasing of MAC (Brown et al., 2018; Wang et al., 2018; Carter et al., 2021), while  
 392 observations or lab experiments mostly link bleaching to the decrease of normalized total absorption coefficient  
 393 (Forrister et al., 2015; Palm et al., 2020; Zeng et al., 2022). It is important to distinguish between these two, because  
 394 the decrease of absorption coefficient can also be caused by loss of absorbing organic material, which will also change  
 395 the scattering coefficient and radiative forcing. Therefore, the MAC of BrC and the absorption coefficient of BrC at  
 396 visible wavelengths were calculated and analyzed together with two chemical clocks (O:C and toluene:benzene ratio)  
 397 and organic mass, to determine whether BrC bleached during the WE-CAN campaign, and whether the bleaching was  
 398 caused by the less organic mass or the changing of refractive index. Because all large wildfire emissions are a mix of  
 399 different regions that are burning slightly different fuels at different combustion efficiencies and because models treat  
 400 regions, not individual fires, we identify relationships in this paper that hold true across all the flight data collected

401 during WE-CAN. These types of broad correlations are much more useful than individual case studies yielding results  
402 that only hold true sometimes.

### 403 3.2.1 Consistency of The Mass Absorption Cross-Section of BrC at 405 nm

404 Palm et al. (2020) combined data from WE-CAN and the Monoterpene and Oxygenated aromatic Oxidation  
405 at Night and under LIGHTs (MOONLIGHT) chamber experiment and found that evaporated biomass-burning POA  
406 is the dominant source of biomass-burning SOA in wildfire plumes during the first a few hours after emission. They  
407 also found that of the SOA formed from oxidation, phenolic compounds contribute  $29 \pm 15\%$  of BrC absorption at  
408 405 nm. In this section, we analyze the characteristics of BrC at 405 nm to understand the average properties of BrC  
409 and to understand the balance of BrC formation versus bleaching during WE-CAN. The MAC of BrC is calculated  
410 following Eq. 4 and therefore it includes a contribution from the lensing effect. The MAC of water-soluble BrC is  
411 calculated following Eq. 5. Figure 3 shows the MAC of BrC at 405 nm versus the aerosol oxidation level (O:C ratio),  
412 while Fig. S2 is a similar plot that uses a simple photochemical clock, the gas-phase toluene:benzene ratio. The O:C  
413 ratio characterizes the oxidation state of OA and typically increases with photochemical age (Aiken et al., 2008), while  
414 the toluene:benzene ratio decreases with photochemical processing time since toluene is more reactive than benzene  
415 (Gouw et al., 2005). Both markers are two commonly used markers to indicate the chemical age of smoke, and they  
416 correlated well with each other during WE-CAN (Fig. S1).

417 The  $MAC_{BrC+lensing\_405}$ , varies from  $0.08 \text{ m}^2 \text{ g}^{-1}$  to  $1.6 \text{ m}^2 \text{ g}^{-1}$  with a mean value of  $0.59 \text{ m}^2 \text{ g}^{-1}$  and a standard  
418 deviation of 0.19. The largest values are from RF05, the flight through California, Oregon, and Idaho, where aged  
419 smoke from different fires was mixed. The large  $MAC_{BrC+lensing\_405}$  occurred when the aircraft left the smoke-filled  
420 boundary layer during RF05. If we exclude  $MAC_{BrC+lensing\_405}$  from RF05, the values range from  $0.08 \text{ m}^2 \text{ g}^{-1}$  to  $1.09$   
421  $\text{m}^2 \text{ g}^{-1}$ , but still have a mean value of  $0.59 \text{ m}^2 \text{ g}^{-1}$  and a standard deviation of 0.15. Again, we note that this value  
422 includes the contribution of lensing. Despite this, our results lie in the same range as those measured without the  
423 contribution of lensing of  $0.31 \pm 0.09 \text{ m}^2 \text{ g}^{-1}$  measured in CLARIFY-2017 (Taylor, 2020),  $0.13\text{-}2.0 \text{ m}^2 \text{ g}^{-1}$  measured  
424 in FIREX-AQ (Zeng et al., 2022), and  $0.25\text{-}1.18 \text{ m}^2 \text{ g}^{-1}$  measured in ORACLES (Zhang et al., 2022). Very weak or  
425 non-trends are observed versus the chemical markers of aging (Fig. 3). If there is any trend, it is a slight increase in  
426  $MAC_{ws\_BrC405}$  with O:C ratio with a poor correlation. A similar weak trend is also observed when compared  
427  $MAC_{ws\_BrC405}$  and  $MAC_{BrC+lensing\_405}$  with the toluene:benzene ratio (Fig. S2). The flat or slightly increasing trend with  
428 increasing oxidation level and decreasing toluene:benzene suggests that the refractive index of BrC is not changing in  
429 a consistent way at 405 nm. It is important to remember that most of the trends observed in WE-CAN are caused by  
430 emissions from different fires versus variations within a single fire, which tend to be quite small. Only 2 flights shows  
431 a clear trend ( $R^2 > 0.3$ ) for both  $MAC_{ws\_BrC405}$  and  $MAC_{BrC+lensing\_405}$  with increasing O:C ratio at the same time, and  
432 they are RF03 ( $R^2$  of 0.85 and 0.85 with positive slope for  $MAC_{ws\_BrC405}$  and  $MAC_{BrC+lensing\_405}$ ), and RF06 ( $R^2$  of 0.8  
433 and 0.49 with negative slope for  $MAC_{ws\_BrC405}$  and  $MAC_{BrC+lensing\_405}$ ), where RF03 only measured a single fire (Taylor  
434 Creek fire).

435

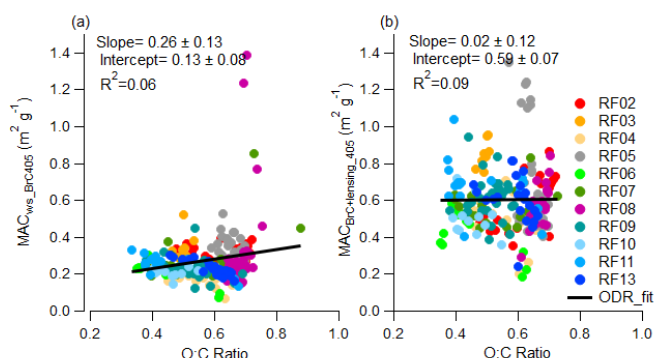


**Figure 3: Plume integrated (a)  $MAC_{ws\_BrC405}$  and (b)  $MAC_{BrC+lensing\_405}$  variations with the organic aerosol O:C ratio**

436 RF05 and RF08 were chosen as case studies, to observe the optical properties of highly aged aerosol to see  
 437 if the optical properties of this aerosol were similar to those observed in the near-field plume sampling of individual  
 438 fires at the longest chemical or physical age observed, which was roughly 6-24 hours of physical aging. RF08 was a  
 439 flight through the Central Valley of California where aged smoke from multiple fires that had settled into the valley  
 440 was measured while RF05 was a flight in which smoke from several California fires was observed in California,  
 441 Oregon and Idaho roughly 300~600 miles from the fires (flightpaths are shown in Fig. 1).  $MAC_{BrC+lensing\_405}$ , CO  
 442 mixing ratio, toluene:benzene ratio, and O:C ratio are displayed in Fig. 4a and 4b. The mixing ratio of CO is relatively  
 443 low in these aged dilute smoke plumes vs. the plumes near the sources analyzed earlier. 1-minute averages of  
 444  $MAC_{BrC+lensing\_405}$  are calculated to reduce noise and 1-minute-averages for toluene:benzene ratio and O:C ratio were  
 445 calculated and all the negative values were removed. As shown in Fig. 4, the smallest toluene:benzene ratio is ~0.35  
 446 in RF05, and is ~0.16 in RF08, while the largest O:C ratio is ~0.7 in both RF05 and RF08, which indicates these two  
 447 cases indeed captured plumes that appear chemically aged to similar extent to the other near-field-source flights where  
 448 the smallest toluene:benzene ratio was 0.33 and the largest O:C ratio was 0.88 in near-fire measurements (Fig. 3, and  
 449 Fig. S2, and Fig S6a).

450 In RF05 (Fig. 4a), the weighted average O:C ratio over the entire flight was 0.64, and the toluene:benzene  
 451 ratio averaged 0.45 with a standard deviation of 0.05.  $MAC_{BrC+lensing\_405}$  varied from  $0.36 \text{ m}^2 \text{ g}^{-1}$  to  $1.52 \text{ m}^2 \text{ g}^{-1}$  with an  
 452 average of  $0.66 \text{ m}^2 \text{ g}^{-1}$  and a standard deviation of  $0.26 \text{ m}^2 \text{ g}^{-1}$ . The plume that was measured in this flight was a  
 453 mixture of different fire sources. Despite the much longer transit time and distance, overall these emissions, which  
 454 were measured 300 to 600 miles away, have a very similar  $MAC_{BrC+lensing\_405}$  to that of the near-source flights where  
 455 we tracked emissions from as near to the fire source as allowed by air traffic control.

456 The RF08 (Fig. 4b) results are similar to RF05, even though these emissions were smoke of mixed aged from  
 457 multiple fire sources in the Central Valley of California. The weighted average O:C ratio was 0.67 over the entire  
 458 measurement, and average toluene:benzene ratio was 0.41 with a standard deviation of 0.15.  $MAC_{BrC+lensing\_405}$   
 459 averaged  $0.59 \text{ m}^2 \text{ g}^{-1}$  with a standard deviation is  $0.14 \text{ m}^2 \text{ g}^{-1}$ . There are several extreme values that exist in the dataset,  
 460 probably because of the SP2 hysteresis time-alignment issues-caused by variation in the dilution rate of the SP2

461 which cannot be totally eliminated from the 1-minute average. In addition, the smoke from RF08 (Fig. 4b) is split into  
 462 four regions based on varying observed CO mixing ratios, and integrated  $MAC_{BrC+lensing\_405}$  is calculated for each  
 463 region (purple star marker). The regional edges are represented by blue dashed lines. Integrated  $MAC_{BrC+lensing\_405}$  for  
 464 all of these variable CO regions is relatively stable with an average value of  $0.59 \text{ m}^2 \text{ g}^{-1}$  and a standard deviation of  
 465  $0.07 \text{ m}^2 \text{ g}^{-1}$ .

466

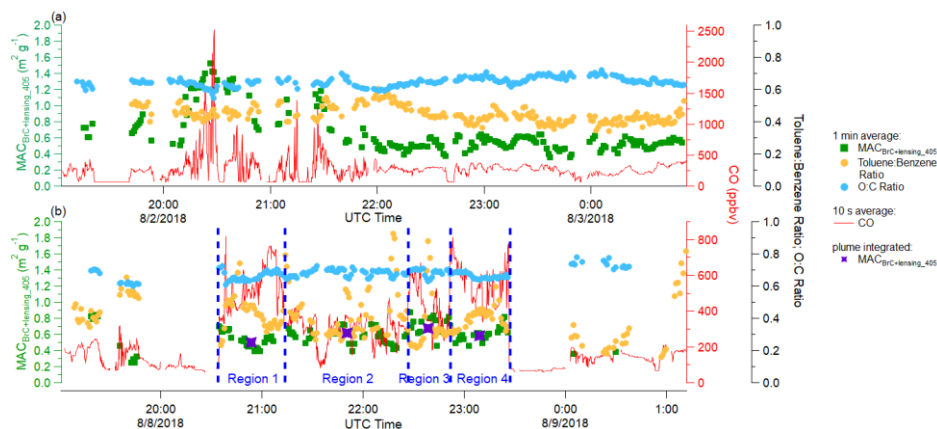


**Figure 4: Time series of plume properties during (a) RF05 (measurements far from fire source), and (b) RF08 (Central Valley of California). Different square and round markers indicate 1 min averages of different variables as shown in the legend, and the red solid line represents 10 s averages of the mixing ratio of CO. Purple stars in RF08 indicate region integrated  $MAC_{BrC+lensing\_405}$  (individual regions are separated based on the concentration of CO, and indicated by blue dashed lines).**

### 467 3.2.2 Decrease in Absorption at 405 nm Observed with Markers of Chemical Oxidation

468 Although neither the  $MAC_{BrC+lensing\_405}$  nor  $MAC_{ws\_BrC405}$  decreases with O:C or Toluene:Benzenes, Fig. 5  
 469 shows that BrC bleaching is observed in terms of decreased total absorption. Figure 5a and 5c show the behavior of  
 470 BrC absorption at 405 nm with markers of the aerosol oxidation level (O:C) and photochemistry (toluene:benzene).  
 471 The absorption coefficient of BrC shown in Fig. 5 is calculated by Eq. 9-10, which cannot separate the absorption  
 472 caused by the BrC and lensing effect. To confirm that observed trends are not the result of changing lensing, the  
 473 absorption coefficient of water-soluble BrC measured by the PILS, which does not include lensing effects, is also  
 474 compared in Fig. 6a and 6c. The average water-soluble BrC absorption at 405 nm ( $Abs_{ws\_BrC405}$ ,  $0.02 \text{ Mm}^{-1} \text{ ppbv}^{-1}$ )  
 475 **which is directly measured by the PILS**, is only 20% of the total absorption from BrC plus lensing ( $Abs_{BrC+lensing\_405}$ ,  
 476  $0.11 \text{ Mm}^{-1} \text{ ppbv}^{-1}$ ), **which is calculated from the PAS and SP2 (Eq.9)**. However,  $Abs_{BrC+lensing\_405}$  and  $Abs_{ws\_BrC405}$   
 477 both decrease with increasing O:C ( $R^2 = 0.65$  and  $R^2 = 0.3$ , respectively for  $Abs_{BrC+lensing\_405}$  and  $Abs_{ws\_BrC405}$ ) and  
 478 decreasing toluene:benzene ratio, which suggest a similar level of decreasing BrC absorption for all the fires observed  
 479 in WE-CAN from numerous locations in the western U.S.. This relationship holds despite differences in fuel type,  
 480 burn conditions, meteorology, etc. between all of these fires. The observed trends are mostly due to the decreasing of



481 both total OA mass (Fig. 5b and 5d) and WSOC (Fig. 6b and 6d) with the increasing O:C ratio ( $R^2 = 0.8$  and  $R^2 = 0.4$ ,  
482 respectively for OA and WSOC) and decreasing toluene:benzene ratio ( $R^2 = 0.64$  and  $R^2 = 0.44$ , respectively for OA  
483 and WSOC). Overall, the organic aerosol O:C ratio better predicts BrC evolution than toluene:benzene ratio, probably  
484 because it is a particle-phase property rather than a gas-phase one. Again, it is important to clarify if BrC “bleaching”  
485 is caused by decreasing BrC absorption coefficient or decreasing of BrC refractive index (or MAC). In this study,  
486 decreasing  $MAC_{BrC}$  is not observed, rather the BrC absorption coefficient decreases significantly with the the simple  
487 O:C and Toluene:Benzenes chemical clocks due to loss of OA mass. Less OA mass also causes decrease in bulk  
488 scattering coefficient (Fig. S3), leading to a very different net radiative effect than reducing  $MAC_{BrC}$ .

489 It is important to recall that we aimed to find general trends that hold for all fires in the western U.S., and the  
490 above trend is significant when all fires are grouped together, although the trend is, in fact, not robust in each flight  
491 and is rather due to variations between the fire plumes rather than variation within a single fire plume. Figure 7 shows  
492 the correlation between normalized OA and chemical age for each fire source. It demonstrates that different fires show  
493 different relationships and that OA does not always decrease with oxidation level/chemical aging within a single fire  
494 (Kiwah fire and Rabbitfoot fire), though increasing O:C ratio does correlate well ( $R^2 > 0.3$ ) with decreasing OA mass  
495 in 7 fires (with  $R^2$  of 0.94 for Taylor Creek fire, 0.87 for Carr fire, 0.86 for Beaver Creek fire, 0.8 for Coal Hollow  
496 fire, 0.76 for Bear Trap fire, 0.35 for Sharps fire, and 0.31 for Sugarloaf fire). Toluene:benzene ratio didn't track OA  
497 as good as O:C ratio, and decreasing toluene:benzene ratio correlates well ( $R^2 > 0.3$ ) with decreasing OA mass in 3  
498 fires (with  $R^2$  of 0.87 for Rabbitfoot fire, 0.85 for Coal Hollow fire, and 0.84 for Bear Trap fire).

499

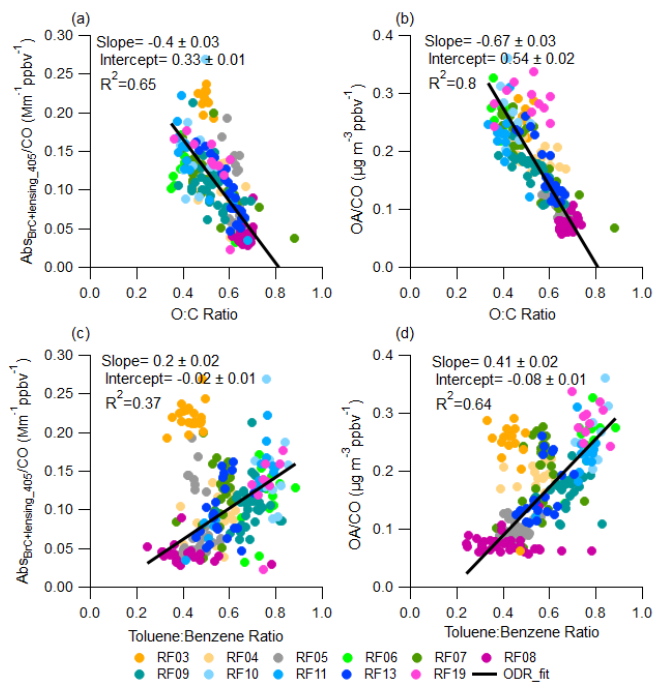


Figure 5: Plume integrated normalized  $Abs_{BrC+lensing\_405}$ , and OA variation with chemical age. Top panels show (a) plume integrated normalized  $Abs_{BrC+lensing\_405}$ , and (b) plume integrated normalized OA variation with O:C ratio. Bottom panels show (c) plume integrated normalized  $Abs_{BrC+lensing\_405}$ , and (d) plume integrated normalized OA variation with toluene:benzene ratio. Data from RF03 was excluded from the ODR fit with toluene:benzene ratio, because RF03 sampled the injection of fresh smoke into the free troposphere, where gas species reacted more rapidly than particles and toluene:benzene ratio failed to keep track of aerosol evolution.

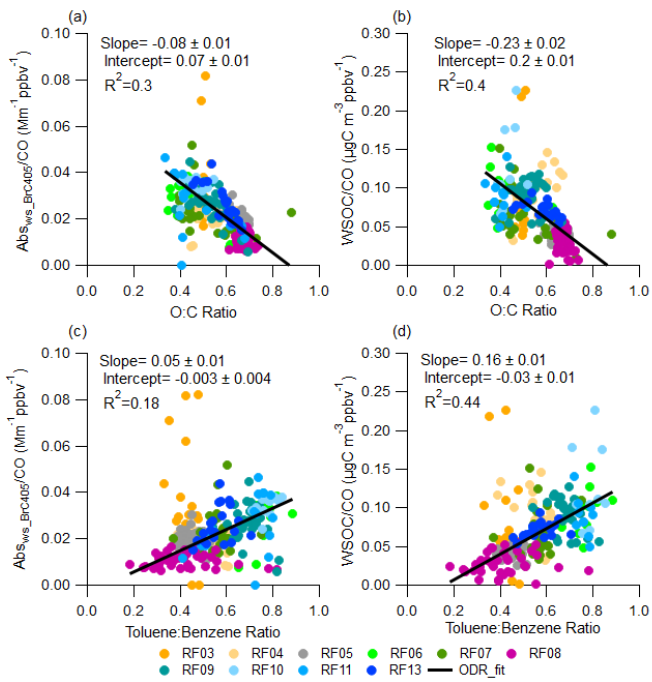


Figure 6: Similar to Fig. 5, but with plume integrated normalized  $Abs_{ws\_BrC405}$  from PILS in (a) and (c), and WSOC in (b) and (d)

501

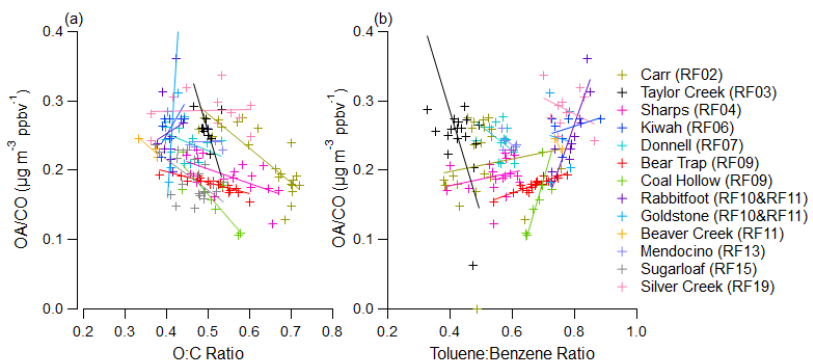


Figure 7: Plume integrated normalized OA variation with (a) O:C ratio and (b) toluene:benzene ratio. Different colors were used to distinguish plumes from different fire sources. Plumes from uncertain fire sources (especially plumes from RF05, RF08) were not included in this plot.

502

503 No trend is observed in CO normalized OA mass with plume physical age (Fig. S4), which is consistent with  
504 the result from Garofalo et al. (2019) in that no net OA mass change was observed in individual plumes during WE-  
505 CAN when they are characterized by physical age, although more data from additional fires were included in the  
506 current work. Plume-integrated CO-normalized OA also shows weak or no trend with altitude and temperature (Fig.  
507 S5). However, we note that the smallest OA:CO was captured in the plumes (RF08) that have highest temperature  
508 (~305 K), and larger OA:CO tends to be observed in the colder plumes (RF19). More studies are needed to determine  
509 how much OA is evaporated in high temperature plumes because the WE-CAN dataset does not capture enough  
510 variation of temperature within plumes to make a robust conclusion. No clear trend was found between  
511  $MAC_{BrC+lensing\_405}$  and physical age or MCE (Fig. S6). Similar behavior was also observed in Western wildfires at 405  
512 nm in FIREX-AQ (Zeng et al., 2022). Part of the reason is that for most fires, we only captured the first few hours (<  
513 15 h), and MCE do not have a robust capability to predict biomass burning particle properties (McClure et al., 2020).  
514 No trend is found between  $MAC_{BrC+lensing\_405}$  and altitude or temperature (Fig. S7). The trend with BC:OA ratio (Fig.  
515 S8) is not as clear as in Saleh et al. (2014), most probably because the range of BC:OA ratios observed during WE-  
516 CAN (0.007~0.061) is much smaller than that (0.005~0.7) observed in Saleh's work. Even in their work, the increasing  
517 trend is not very clear if one only focuses on the region where the BC:OA ratio is less than 0.03. Also, the Saleh et al.  
518 (2014) results were obtained from laboratory burns and not wildfires, which might also cause a discrepancy.

### 519 3.2.3 Mass Absorption Cross-Section and Optical Properties of BrC at 660 nm

520 BrC is defined as OA that has strong absorption at UV and shorter visible portions of the spectrum and has  
521 been historically considered to be almost transparent near the red wavelengths (Andreae and Gelencsér, 2006; Bahadur  
522 et al., 2012; Liu et al., 2020). However, during WE-CAN, we were able to quantify  $Abs_{ws\_BrC660}$  with the PILS  
523 instrument. We know that absorption observed in the PILS at 660 nm is not BC because BC is insoluble and will be  
524 removed by [the PILS impactor](#), the 0.2  $\mu\text{m}$  filter in the instrument, [and that BC over 110 nm in size will not be oxidized](#)  
525 [by the TOC analyzer \(Peltier et al., 2007; Zeng et al., 2021; Sullivan et al., 2022\)](#). Next, we investigate the behavior  
526 of BrC absorption at 660 nm to see if BrC has a similar behavior at the long versus short ends of the visible spectrum.

527 Figure 8 shows the behavior of brown carbon at 660 nm vs. the O:C ratio. Similar to 405 nm, no bleaching  
528 in terms of decreased MAC is observed at 660 nm. If there is any trend, it is increasing  $MAC_{ws\_BrC660}$  and  
529  $MAC_{BrC+lensing\_660}$  with organic aerosol O:C ratio. Similar trends are observed, though with lower correlation, versus  
530 the toluene:benzene ratio (Fig. S9). The mean value of  $MAC_{BrC+lensing\_660}$  is  $0.11 \text{ m}^2 \text{ g}^{-1}$  (with a standard deviation of  
531 0.06), which is much larger than the 0.03 average of  $MAC_{ws\_BrC660}$ , a result we have attributed to the lensing effect,  
532 but which could also partially be the result of water-insoluble BrC having a higher MAC than water-soluble BrC.

533 These results for the behavior of  $MAC_{BrC}$  at different wavelengths derived using different instruments (PAS  
534 and PILS) is further evidence that  $MAC_{BrC}$  does not decrease with physical or chemical age in the WE-CAN dataset.  
535 At a minimum, the plume integrated results, which represent total optical properties relevant to climate models, do  
536 not capture any  $MAC_{BrC}$  decay that might be occurring at the edges of the plume.

537

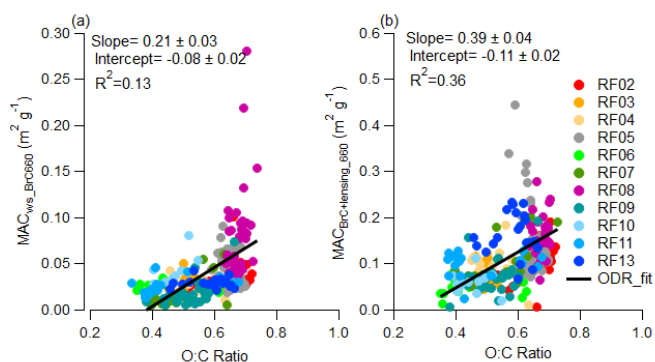


**Figure 8: Plume integrated (a)  $MAC_{ws\_BrC660}$  and (b)  $MAC_{BrC+lensing\_660}$  variations with O:C ratio**

538 Similar to our analysis at 405 nm, RF05 and RF08 are presented as case studies to investigate the behavior  
 539 of  $MAC_{BrC+lensing\_660}$  in aged plumes emitted from different fire sources. Figure 9 is similar to Fig. 4, but with  
 540  $MAC_{BrC+lensing\_660}$  instead of  $MAC_{BrC+lensing\_405}$ . For the case of RF05 (Fig. 9a)  $MAC_{BrC+lensing\_660}$  varied from 0.04  $m^2$   
 541  $g^{-1}$  to 0.40  $m^2 g^{-1}$  with an average of 0.15  $m^2 g^{-1}$  and a standard deviation of 0.07  $m^2 g^{-1}$ . The  $MAC_{BrC+lensing\_660}$  tends  
 542 to be larger when CO mixing ratio is higher, but does not have a significant correlation with any marker of oxidation  
 543 level or photochemistry shown in Fig. 9. For the case of RF08 (Fig. 9b)  $MAC_{BrC+lensing\_660}$  is more stable than in RF05,  
 544 and varied from 0.04  $m^2 g^{-1}$  to 0.37  $m^2 g^{-1}$  with an average of 0.18  $m^2 g^{-1}$  and a standard deviation of 0.06  $m^2 g^{-1}$ . The  
 545 regional integrated  $MAC_{BrC+lensing\_660}$  is even more stable with an average value of 0.16  $m^2 g^{-1}$  and a standard deviation  
 546 of 0.01  $m^2 g^{-1}$ . Similar to the results at 405 nm, we observe that the MAC in these very aged plumes is very similar to  
 547 the average MAC observed in the near field.  
 548

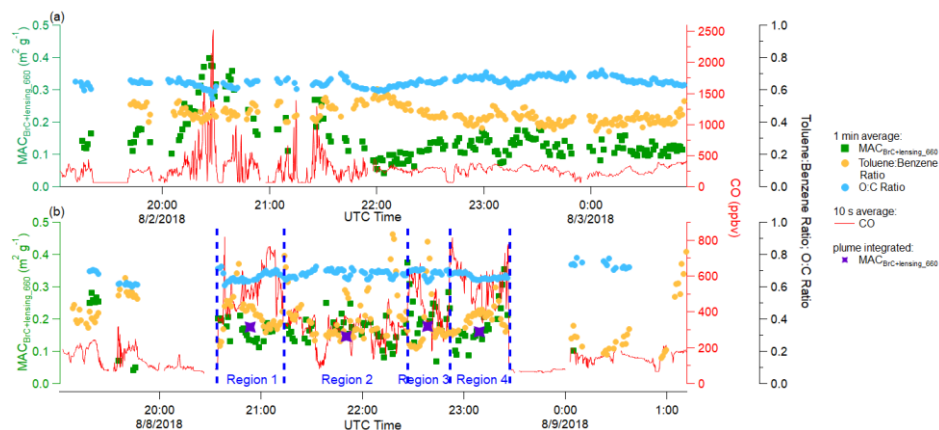


**Figure 9: Time series of plume properties during (a) RF05, and (b) RF08(Central Valley of California). Different square and round markers indicate 1 min averages of different variables as shown in the legend, and the red solid line represents 10 s averages of the mixing ratio of CO. Purple stars in RF08 indicate region integrated  $MAC_{BrC+lensing\_660}$  (individual regions are separated based on the concentration of CO, and indicated by blue dashed lines).**

549 Normalized  $Abs_{BrC+lensing\_660}$  and total scattering coefficient at 660 nm (Fig. S10), as well as normalized  
 550  $Abs_{ws\_BrC660}$  (Fig. S11) were also investigated to see if they decreased with markers of chemical age similar to the  
 551 results seen at 405 nm. However, the correlation between these BrC optical properties with O:C ratio or  
 552 toluene:benzene ratio at 660 nm is much weaker and flatter than they are at 405 nm. Perhaps this is because BrC  
 553 absorption is very small at 660 nm, and a large uncertainty is brought in from the assumptions required for calculation  
 554 of this property and instrumental uncertainties. The average normalized  $Abs_{BrC+lensing\_660}$  is  $0.02 \text{ Mm}^{-1} \text{ ppbv}^{-1}$ , which  
 555 is 5 times lower than the absorption at 405 nm; while the average normalized  $Abs_{ws\_BrC660}$  is an order of magnitude  
 556 lower than  $Abs_{ws\_BrC405}$ . The  $MAC_{BrC+lensing\_660}$  (Fig. S12) shows better correlation with BC:OA ratio than  
 557  $MAC_{BrC+lensing\_405}$ , though the increasing trend is still not as significant as Saleh et al. (2014) due to a much smaller  
 558 BC:OA ratio during WE-CAN.

### 559 3.3 Relative Importance of BrC vs. the Lensing Effect at 660 nm

560 Plume integrated  $MAC_{BC}$  at 660 nm ( $MAC_{BC660}$ ) from the 13 WE-CAN research flights with clear plume  
 561 transects of biomass burning plumes are shown in Fig. 10. The  $MAC_{BC660}$  discussed in this section is calculated from  
 562 Eq. 3, and has contributions from absorption from the BC core, the BrC shell, and the lensing effect. Again, even fire  
 563 plumes from individually named fires are usually a mix of many different burning conditions, and it is hard to identify  
 564 the exact source in most wildfire smoke measurements, especially for well mixed plumes. Therefore flight-to-flight  
 565 data is analyzed because each flight covered a region, and an overall behavior of absorbing aerosol from wildfire can  
 566 be provided.  $MAC_{BC660}$  varies between different flights with RF03 having the highest average  $MAC_{BC660}$  of  $12.9 \text{ m}^2$   
 567  $\text{g}^{-1}$ , and RF10 having the lowest average  $MAC_{BC660}$  of  $8.6 \text{ m}^2 \text{ g}^{-1}$ . Even in highly aged plumes with emissions mixed  
 568 from multiple fires (RF05 and RF08), the  $MAC_{BC660}$  is similar in magnitude and consistency with an average of  $11.3$

569  $\pm 1.8 \text{ m}^2 \text{ g}^{-1}$ . The average of all plume-integrated  $\text{MAC}_{\text{BC660}}$  is  $10.9 \text{ m}^2 \text{ g}^{-1}$ , with a standard deviation of  $2.1 \text{ m}^2 \text{ g}^{-1}$ .  
 570 This result is similar to some other recent airborne measurements. Subramanian et al. (2010) reported a  $\text{MAC}_{\text{BC660}}$  of  
 571  $10.9 \pm 2.1 \text{ m}^2 \text{ g}^{-1}$  using a SP2 and PSAP operated during the MILAGRO campaign, which included airborne  
 572 measurements of biomass burning over Mexico. Similarly, Zhang et al. (2017) estimated a  $\text{MAC}_{\text{BC660}}$  of  $10 \text{ m}^2 \text{ g}^{-1}$   
 573 utilizing both SP2 and PSAP deployed on the NASA DC-8 research aircraft for the DC3 campaign, which measured  
 574 the upper tropospheric BC over the central U.S. Taylor et al. (2020) calculated a  $\text{MAC}_{\text{BC655}}$  of  $12 \pm 2 \text{ m}^2 \text{ g}^{-1}$  for biomass  
 575 burning emissions from Africa over the southeast Atlantic Ocean, using airborne measurements from a SP2 and PAS  
 576 in the CLARIFY-2017 campaign.

577 These results are encouragingly similar given the breadth of measurement techniques (PSAP is filter-based  
 578 whereas PAS is a direct measurement), geographic regions (Continental U.S. for DC3, Mexico for MILAGRO, African  
 579 outflow for CLARIFY) and altitude in the atmosphere (all were airborne campaigns covering a range of altitudes). If  
 580 we apply  $6.3 \text{ m}^2 \text{ g}^{-1}$  as the MAC of a BC core at 660 nm (Bond and Bergstrom, 2006; Subramanian et al., 2010), then  
 581 the average absorption enhancement for the entire WE-CAN campaign is 1.7. This means the absorption of coated BC  
 582 is 1.7 times higher than bare BC at 660 nm, which is somewhat close to the factor of  $\sim 2$  reported by laboratory  
 583 experiments (Schnaiter et al., 2005; Peng et al., 2016), larger than some field measurements (Cappa et al., 2012&2019;  
 584 Healy et al., 2015), but close to  $1.85 \pm 0.45$  measured by Taylor et al. (2020) in African biomass burning plumes. The  
 585 similarity to the Taylor et al. (2020) result suggests global similarities in the  $\text{MAC}_{\text{BC660}}$  from aerosol emitted from  
 586 wildfires.

587

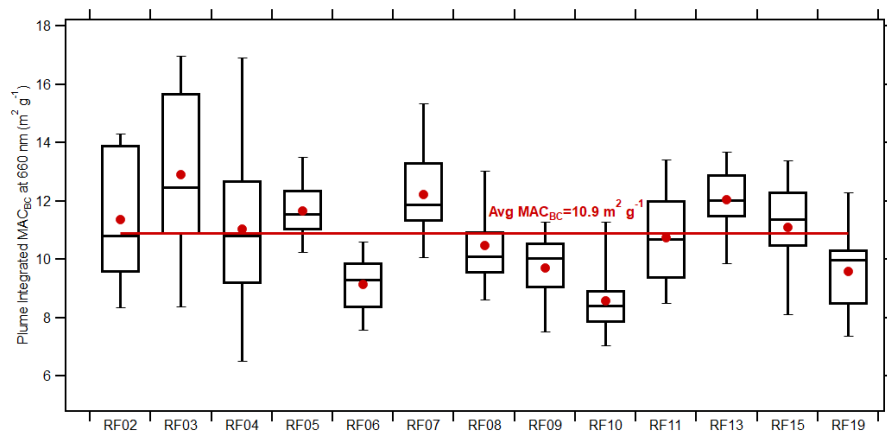


**Figure 10: Box plots of plume integrated  $\text{MAC}_{\text{BC660}}$  for each flight. On each box the central line represents the median, the top and bottom edges represent the 75<sup>th</sup> and 25<sup>th</sup> percentile, and the top and bottom whiskers represent the 90<sup>th</sup> and 10<sup>th</sup> percentile of the data. The red dot shows the average, and the red line indicates the average value for all plume integrated  $\text{MAC}_{\text{BC660}}$ .**

588  $MAC_{BC660}$  is also compared with the physical age and MCE (Fig. S13), the O:C and toluene:benzene chemical  
589 clocks (Fig. S14), and the altitude, temperature and dilution ( $\Delta CO$ ) (Fig. S15). However, no clear trend is be found in  
590 these comparisons.

591 The average absorption enhancement of 1.7 at 660 nm in this study indicates that, on average, 41% of total  
592 absorption at 660 nm is caused by lensing and absorbing organics, instead of BC itself. Figure 11 shows the fraction  
593 of non-BC absorption from BrC at 660 nm for the biomass burning plumes encountered during WE-CAN using Eq.  
594 6-8 with OM calculated from the AMS. The figure is plotted versus plume physical age to allow visualization of the  
595 variability, though there is no clear trend with physical age other than perhaps a decrease in variability with increasing  
596 physical age. Figure S16 shows a similar result by using OM calculated from the UHSAS. More details on the  
597 calculation and the AMS vs. UHSAS methods are explained in section 2.5. Assuming a MAC of the BC core of 6.3  
598  $m^2 g^{-1}$ , BrC contributes roughly the same amount of absorption at 660 nm as lensing (46% from the AMS method, 62%  
599 from the UHSAS method). This means that 19% (AMS method) to 26% (UHSAS method) of the total absorption at  
600 660 nm comes from BrC. When different particle density and WSOM:WSOC ratios are considered (top and bottom  
601 whiskers, as well as red and blue dashed lines), the fraction of non-BC absorption is 41-49% for the AMS approach  
602 (Fig. 11) and 43-80% for the UHSAS approach (Fig. S16) based on different OM:OC and density. The UHSAS  
603 approach shows larger uncertainty because it's sensitive to the particle density when calculating particulate mass  
604 (Table S1). While there is considerable variability between flights, a rule of thumb that roughly half of the non-BC  
605 absorption at red wavelengths is from absorbing organic material seems reasonable. To the best of our knowledge, this  
606 is the first observation-based attempt to differentiate between lensing and absorbing organics in the red wavelengths.  
607 This approach assumes that water insoluble BrC has the same refractive index as water soluble BrC.

608



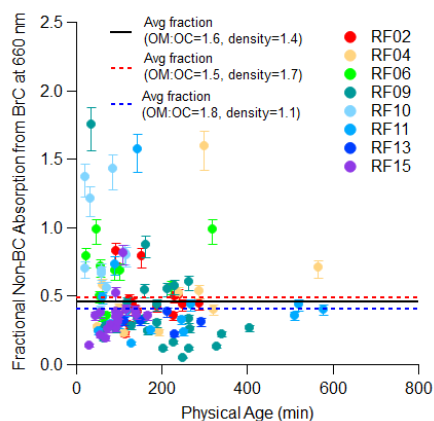


Figure 11: Time evolution of the fraction of non-BC absorption from BrC at 660 nm with AMS and Mie factor. Markers were calculated using a density of  $1.4 \text{ g cm}^{-3}$  and WSOM:WSOC ratio of 1.6. The top whiskers represent sensitive test values using a density of  $1.7 \text{ g cm}^{-3}$  and WSOM:WSOC ratio of 1.5, while the bottom whiskers represent sensitive test values using a density of  $1.1 \text{ g cm}^{-3}$  and WSOM:WSOC ratio of 1.8. The averaged fraction of non-BC absorption from BrC from all the plumes are shown in black solid lines, while the range of this result from sensitivity tests are shown in red and blue dashed lines.

#### 609 4 Conclusion

610 In this study, we presented results that enable a better understanding of the ability of aerosol emissions from  
 611 wildfires to absorb visible light and how those properties change after emission. We presented mass absorption  
 612 coefficients (MAC) for BC and BrC from Western United States wildfires measured during the WE-CAN campaign  
 613 at both short and long visible wavelengths ( $\text{MAC}_{\text{BC}660}$ ,  $\text{MAC}_{\text{BrC+lensing}_660}$ ,  $\text{MAC}_{\text{ws}_\text{BrC}660}$ ,  $\text{MAC}_{\text{BrC+lensing}_405}$ ). We also  
 614 investigated the bulk absorption coefficient for BrC and bulk scattering coefficient for total aerosol at both short and  
 615 long visible wavelengths. General trends that held for all the fire sources are derived, which should be valid throughout  
 616 the western U.S. given the wide variety of emissions used to develop them.

617 By utilizing a common parameterization for BrC refractive index from Saleh et al. (2014), with measured  
 618 inputs for the BC:OA ratio and particle size, we calculated the theoretical  $\text{MAC}_{\text{BrC}660}$  and  $\text{MAC}_{\text{BrC}405}$ , and they were  
 619 2.3–3.4 times larger than the measured  $\text{MAC}_{\text{BrC+lensing}}$  during WE-CAN. While this discrepancy has been resolved  
 620 previously by implementing bleaching into model schemes, we show that this is probably the incorrect explanation  
 621 given the MAC of BrC either remains constant or slightly increases when chemical markers (O:C, toluene:benzene)  
 622 suggest more oxidation has occurred. We suggest a different parameterization of the refractive index is needed to  
 623 represent wildfire optical properties in the Western United States rather than using bleaching to decrease the mass  
 624 absorption cross section (MAC) of the Saleh parameterization. We also note that there needs to be better terminology  
 625 to distinguish between decreasing absorption caused by losses of organic aerosol mass versus decreasing absorption  
 626 caused by changes in the MAC of the aerosol.

627 In the blue visible wavelengths, where BrC is more often thought about,  $MAC_{BrC+lensing\_405}$  is  $0.59 \pm 0.19 \text{ m}^2$   
628  $\text{g}^{-1}$  and shows little variation with physical age, MCE, altitude, temperature or BC:OA ratio. There isn't any decreasing  
629 trends in all the  $MAC_{BrC}$  data we obtained ( $MAC_{ws\_BrC405}$ ,  $MAC_{BrC+lensing\_405}$ ,  $MAC_{ws\_BrC660}$ , and  $MAC_{BrC+lensing\_660}$ )  
630 with markers of chemical age (toluene:benzene, O:C), but bulk absorption of BrC does decrease with these same  
631 markers. In highly aged plumes from multiple fires (RF05 and RF08), the  $MAC_{BrC+lensing\_405}$  has an average value of  
632  $0.63 \pm 0.2 \text{ m}^2 \text{ g}^{-1}$ , suggesting that brown carbon remains significantly absorbing even at relatively longer ages.

633 We find that total organic aerosol (OA) and water-soluble organic carbon (WSOC) are strongly correlated  
634 with chemical markers of oxidative age. OA and WSOC (both normalized to CO) decrease with decreasing  
635 toluene:benzene ratio and increasing O:C ratio. However, this phenomenon is only clearly observed when data from  
636 all the observed fires is included rather than during the aging of individual fire plumes. This could mean that the fires  
637 either had different emission ratios of toluene:benzene and O:C or the smoke underwent rapid secondary chemistry  
638 prior to the first plume pass in WE-CAN. Regardless, the correlations are fairly robust ( $R^2$  of 0.4 to 0.8) given the  
639 many variables (MCE, fuel type, etc.) that are changing in the dataset and provide a potential link between chemical  
640 markers and total organic aerosol amounts across a wide range of fires. While OA and WSOC decrease with decreasing  
641 toluene:benzene or increasing O:C,  $MAC_{BrC}$  actually shows a weak increasing trend with these same markers of aging,  
642 showing that while the total amount of organic aerosol is decreasing, the ability of the organic to absorb per mass is  
643 staying relatively constant, or even increasing. We also found that the bulk scattering coefficient (normalized to CO)  
644 decreases with decreasing toluene:benzene ratio or increasing O:C ratio due to less OA being present, which leads to  
645 a very different net radiative effect than that which results from just changing the refractive index of BrC.

646 In the red visible wavelengths, where BrC is often less noticed, we observed that the MAC of BC stayed  
647 relatively constant across all plumes measured and at all physical ages (ages up to 15 hours observed), with an averaged  
648  $MAC_{BC660}$  of  $10.9 \pm 2.1 \text{ m}^2 \text{ g}^{-1}$  (average  $\pm$  standard deviation), which includes the contribution from both lensing effect  
649 and absorbing organics. This average showed no clear trends with altitude or temperature, and we saw no evidence  
650 that  $MAC_{BC660}$  is correlated to MCE. Even in highly aged plumes with emissions mixed from multiple fires (RF05  
651 and RF08), the  $MAC_{BC660}$  is similar in magnitude to the near-source plumes with an average of  $11.3 \pm 1.8 \text{ m}^2 \text{ g}^{-1}$ . Both  
652 the fact that this MAC is significantly larger than the MAC for uncoated BC (often cited to be  $\sim 6.3 \text{ m}^2 \text{ g}^{-1}$ ) and the  
653 fact that the MAC remains relatively constant across different fires and different plume ages are key insights that can  
654 improve models of aerosol optical properties in wildfire emissions.

655 Through a novel use of PILS data, we find that BrC contributes 41-80% of non-BC absorption at 660 nm  
656 (assuming  $6.3 \text{ m}^2 \text{ g}^{-1}$  as the MAC of BC core at 660 nm). BrC contributes, on average, 26% of total absorption, but  
657 the absorption cross section of water-soluble BrC is relatively small at 660 nm, with a  $MAC_{ws\_BrC660}$  of  $0.03 \pm 0.02 \text{ m}^2$   
658  $\text{g}^{-1}$ , which does not change with physical age, and no trend with MCE is observed. The average  $MAC_{BrC+lensing\_660}$   
659 derived from the PAS (which includes both brown carbon absorption and lensing of black carbon) is  $0.11 \pm 0.06 \text{ m}^2$   
660  $\text{g}^{-1}$ .

#### 661 **Data Availability**

662 The WE-CAN data can be found at [http://data.eol.ucar.edu/master\\_lists/generated/we-can/](http://data.eol.ucar.edu/master_lists/generated/we-can/).

663 The DOI for each data set used in this work are:

664 PAS and CAPS PM<sub>SSA</sub>: <https://doi.org/10.26023/K8P0-X4T3-TN06>

665 PILS1: <https://doi.org/10.26023/9H07-MD9K-430D> and <https://doi.org/10.26023/CRHY-NDT9-C30V>

666 PILS2: <https://doi.org/10.26023/7TAN-TZMD-680Y>

667 SP2: <https://doi.org/10.26023/P8R2-RAB6-N814>

668 UHSAS: <https://doi.org/10.26023/BZ4F-EAC4-290W>

669 PTR-ToF-MS: <https://doi.org/10.26023/K9F4-2CNH-EQ0W>

670 HR-AMS: <https://doi.org/10.26023/MM2Y-ZGFQ-RB0B>

671 Picarro: <https://doi.org/10.26023/NNYM-Z18J-PX0Q>

672 miniQCL: <https://doi.org/10.26023/Q888-WZRD-B70F>

### 673 **Author Contributions**

674 SMM designed the project. YS wrote the paper. YS, RPP, APS, EJTL, LAG, DKF, WP, LH, DWT, TC, EVF, and SMM  
675 collected and analyzed data.

### 676 **Competing Interests**

677 The authors declare that they have no conflict of interest.

### 678 **Acknowledgements**

679 The 2018 WE-CAN field campaign was supported by the U.S. National Science Foundation through grants AGS-  
680 1650493 (U of Wyoming), AGS-1650786 (Colorado State U), AGS-1650275 (U of Montana), AGS-1650288 (U of  
681 Colorado at Boulder), and the National Oceanic and Atmospheric Administration (Award # NA17OAR4310010,  
682 Colorado State U). This material is based upon study supported by the National Center for Atmospheric Research,  
683 which is a major facility sponsored by the National Science Foundation under Cooperative Agreement no. 1852977.  
684 The authors acknowledge support from AGS-1650493 for YS, SMM and RPP, AGS-1650786 for APS and EJTL,  
685 AGS-2144896 for LH and WP, AGS-1650288 for DWT, NOAA Climate Program Office's Atmospheric Chemistry,  
686 Carbon Cycle, and Climate program (Grant NA17OAR4310010) for DKF and LAG.

687

688 We sincerely thank Ernie Lewis for his work implementing Mie theory into Igor code.

### 689 **References**

690 [Aiken, A. C., Decarlo, P. F., Kroll, J. H., Worsnop, D. R., Huffman, J. A., Docherty, K. S., Ulbrich, I. M., Mohr, C.,](#)  
691 [Kimmel, J. R., Sueper, D., Sun, Y., Zhang, Q., Trimbom, A., Northway, M., Ziemann, P. J., Canagaratna, M. R.,](#)  
692 [Onasch, T. B., Alfarra, M. R., Prevot, A. S. H., Dommen, J., Duplissy, J., Metzger, A., Baltensperger, U. and](#)

693 [Jimenez, J. L.: O/C and OM/OC ratios of primary, secondary, and ambient organic aerosols with high-resolution](#)  
694 [time-of-flight aerosol mass spectrometry, \*Environ. Sci. Technol.\*, 42\(12\), 4478–4485, doi:10.1021/es703009q,](#)  
695 [2008.](#)

696 [Akagi, S. K., Yokelson, R. J., Wiedinmyer, C., Alvarado, M. J., Reid, J. S., Karl, T., Crouse, J. D. and Wennberg, P.](#)  
697 [O.: Emission factors for open and domestic biomass burning for use in atmospheric models, \*Atmos. Chem. Phys.\*,](#)  
698 [11\(9\), 4039–4072, doi:10.5194/acp-11-4039-2011, 2011.](#)

699 [Andreae, M. O.: Emission of trace gases and aerosols from biomass burning – An updated assessment, \*Atmos. Chem.\*  
700 \[Phys. Discuss., 1–27, doi:10.5194/acp-2019-303, 2019.\]\(#\)](#)

701 [Andreae, M. O. and Gelencsér, A.: Black carbon or brown carbon? The nature of light-absorbing carbonaceous](#)  
702 [aerosols, \*Atmos. Chem. Phys.\*, 6, 3131–3148, doi:10.5194/acp-6-3131-2006, 2006.](#)

703 [Bahadur, R., Praveen, P. S., Xu, Y. and Ramanathan, V.: Solar absorption by elemental and brown carbon determined](#)  
704 [from spectral observations, \*Proc. Natl. Acad. Sci.\*, 109\(43\), 17366–17371, doi:10.1073/pnas.1205910109, 2012.](#)

705 [Bohren, C. F. and Huffman, D. R.: Absorption and scattering of light by small particles., 1983.](#)

706 [Bond, T. C. and Bergstrom, R. W.: Light absorption by carbonaceous particles: An investigative review, \*Aerosol Sci.\*  
707 \[Technol., 40\\(1\\), 27–67, doi:10.1080/02786820500421521, 2006.\]\(#\)](#)

708 [Bond, T. C., Habib, G. and Bergstrom, R. W.: Limitations in the enhancement of visible light absorption due to mixing](#)  
709 [state, \*J. Geophys. Res. Atmos.\*, 111\(20\), 1–13, doi:10.1029/2006JD007315, 2006.](#)

710 [Bond, T. C., Doherty, S. J., Fahey, D. W., Forster, P. M., Berntsen, T., Deangelo, B. J., Flanner, M. G., Ghan, S.,](#)  
711 [Kärcher, B., Koch, D., Kinne, S., Kondo, Y., Quinn, P. K., Sarofim, M. C., Schultz, M. G., Schulz, M.,](#)  
712 [Venkataraman, C., Zhang, H., Zhang, S., Bellouin, N., Guttikunda, S. K., Hopke, P. K., Jacobson, M. Z., Kaiser, J.](#)  
713 [W., Klimont, Z., Lohmann, U., Schwarz, J. P., Shindell, D., Storelvmo, T., Warren, S. G. and Zender, C. S.:](#)  
714 [Bounding the role of black carbon in the climate system: A scientific assessment, \*J. Geophys. Res. Atmos.\*, 118\(11\),](#)  
715 [5380–5552, doi:10.1002/jgrd.50171, 2013.](#)

716 [Brown, H., Liu, X., Feng, Y., Jiang, Y., Wu, M., Lu, Z., Wu, C., Murphy, S. and Pokhrel, R.: Radiative effect and](#)  
717 [climate impacts of brown carbon with the Community Atmosphere Model \(CAM5\), \*Atmos. Chem. Phys.\*, 18\(24\),](#)  
718 [17745–17768, doi:10.5194/acp-18-17745-2018, 2018.](#)

719 [Brown, H., Liu, X., Pokhrel, R., Murphy, S., Lu, Z., Saleh, R., Mielonen, T., Kokkola, H., Bergman, T., Myhre, G.,](#)  
720 [Skeie, R. B., Watson-Paris, D., Stier, P., Johnson, B., Bellouin, N., Schulz, M., Vakkari, V., Beukes, J. P., van Zyl,](#)  
721 [P. G., Liu, S. and Chand, D.: Biomass burning aerosols in most climate models are too absorbing, \*Nat. Commun.\*,](#)  
722 [12\(1\), 1–15, doi:10.1038/s41467-020-20482-9, 2021.](#)

723 [Burke, M., Driscoll, A., Heft-Neal, S., Xue, J., Burney, J. and Wara, M.: The changing risk and burden of wildfire in](#)  
724 [the United States, \*Proc. Natl. Acad. Sci. U. S. A.\*, 118\(2\), 1–6, doi:10.1073/PNAS.2011048118, 2021.](#)

725 [Canagaratna, M. R., Jimenez, J. L., Kroll, J. H., Chen, Q., Kessler, S. H., Massoli, P., Hildebrandt Ruiz, L., Fortner,](#)  
726 [E., Williams, L. R., Wilson, K. R., Surratt, J. D., Donahue, N. M., Jayne, J. T. and Worsnop, D. R.: Elemental ratio](#)  
727 [measurements of organic compounds using aerosol mass spectrometry : characterization , improved calibration ,](#)  
728 [and implications, \*Atmos. Chem. Phys.\*, 15\(1\), 253–272, doi:10.5194/acp-15-253-2015, 2015.](#)

729 [Cappa, C. D., Onasch, T. B., Massoli, P., Worsnop, D. R., Bates, T. S., Cross, E. S., Davidovits, P., Hakala, J., Hayden,](#)  
730 [K. L., Jobson, B. T., Kolesar, K. R., Lack, D. A., Lerner, B. M., Li, S. M., Mellon, D., Nuaaman, I., Olfert, J. S.,](#)  
731 [Petäjä, T., Quinn, P. K., Song, C., Subramanian, R., Williams, E. J. and Zaveri, R. A.: Radiative absorption](#)  
732 [enhancements due to the mixing state of atmospheric black carbon, \*Science\* \(80- \), 337\(6098\), 1078–1081,](#)  
733 [doi:10.1126/science.1223447, 2012.](#)

734 [Cappa, C. D., Zhang, X., Russell, L. M., Collier, S., Lee, A. K. Y., Chen, C. L., Betha, R., Chen, S., Liu, J., Price, D.](#)  
735 [J., Sanchez, K. J., McMeeking, G. R., Williams, L. R., Onasch, T. B., Worsnop, D. R., Abbatt, J. and Zhang, Q.:](#)  
736 [Light Absorption by Ambient Black and Brown Carbon and its Dependence on Black Carbon Coating State for](#)  
737 [Two California, USA, Cities in Winter and Summer, \*J. Geophys. Res. Atmos.\*, 124\(3\), 1550–1577,](#)  
738 [doi:10.1029/2018JD029501, 2019.](#)

739 [Carter, T. S., Heald, C. L., Cappa, C. D., Kroll, J. H., Campos, T. L., Coe, H., Cotterell, M. I., Davies, N. W., Farmer,](#)  
740 [D. K., Fox, C., Garofalo, L. A., Hu, L., Langridge, J. M., Levin, E. J. T., Murphy, S., Pöhlrel, R., Shen, Y., Szpek,](#)  
741 [K., Taylor, J. W. and Wu, H.: Investigating Carbonaceous Aerosol and its Absorption Properties from Fires in the](#)  
742 [western US \(WE-CAN\) and southern Africa \(ORACLES and CLARIFY\), \*J. Geophys. Res. Atmos.\*, 1–28,](#)  
743 [doi:10.1029/2021JD034984, 2021.](#)

744 [Chen, M., Sun, Z., Davis, J. M., Liu, Y. A., Corr, C. A. and Gao, W.: Improving the mean and uncertainty of ultraviolet](#)  
745 [multi-filter rotating shadowband radiometer in situ calibration factors: Utilizing Gaussian process regression with](#)  
746 [a new method to estimate dynamic input uncertainty, \*Atmos. Meas. Tech.\*, 12\(2\), 935–953, doi:10.5194/amt-12-](#)  
747 [935-2019, 2019.](#)

748 [Cho, C., Kim, S. W., Lee, M., Lim, S., Fang, W., Gustafsson, Ö., Andersson, A., Park, R. J. and Sheridan, P. J.:](#)  
749 [Observation-based estimates of the mass absorption cross-section of black and brown carbon and their contribution](#)  
750 [to aerosol light absorption in East Asia, \*Atmos. Environ.\*, 212\(November 2018\), 65–74,](#)  
751 [doi:10.1016/j.atmosenv.2019.05.024, 2019.](#)

752 [Craig, L., Moharreri, A., Schanot, A., Rogers, D. C., Dhaniyala, S., Craig, L., Anderson, B. and Dhaniyala, S.:](#)  
753 [Characterizations of Cloud Droplet Shatter Artifacts in Two Airborne Aerosol Inlets, \*Aerosol Sci. Technol.\*, 47:6,](#)  
754 [662–671, doi:10.1080/02786826.2013.780648, 2013a.](#)

755 [Craig, L., Schanot, A., Moharreri, A., Rogers, D. C. and Dhaniyala, S.: Design and Sampling Characteristics of a New](#)  
756 [Airborne Aerosol Inlet for Aerosol Measurements in Clouds, \*J. Atmos. Ocean. Technol.\*, 30, 1123–1135,](#)  
757 [doi:10.1175/JTECH-D-12-00168.1, 2013b.](#)

758 [Duarte, R. M. B. O., Freire, S. M. S. C. and Duarte, A. C.: Investigating the water-soluble organic functionality of](#)  
759 [urban aerosols using two-dimensional correlation of solid-state <sup>13</sup>C NMR and FTIR spectral data, \*Atmos. Environ.\*,](#)  
760 [116, 245–252, doi:10.1016/j.atmosenv.2015.06.043, 2015.](#)

761 [Duarte, R. M. B. O., Piñeiro-Iglesias, M., López-Mahía, P., Muniategui-Lorenzo, S., Moreda-Piñeiro, J., Silva, A. M.](#)  
762 [S. and Duarte, A. C.: Comparative study of atmospheric water-soluble organic aerosols composition in contrasting](#)  
763 [suburban environments in the Iberian Peninsula Coast, \*Sci. Total Environ.\*, 648, 430–441,](#)  
764 [doi:10.1016/j.scitotenv.2018.08.171, 2019.](#)

765 [Eatough, D. J., Wadsworth, A., Eatough, D. A., Crawford, J. W., Hansen, L. D. and Lewis, E. A.: A multiple-system,](#)  
766 [multi-channel diffusion denuder sampler for the determination of fine-particulate organic material in the](#)  
767 [atmosphere. \*Atmos. Environ. Part A, Gen. Top.\*, 27\(8\), 1213–1219, doi:10.1016/0960-1686\(93\)90247-V, 1993.](#)

768 [Finessi, E., Decesari, S., Paglione, M., Giulianelli, L., Carbone, C., Gilardoni, S., Fuzzi, S., Saarikoski, S., Raatikainen,](#)  
769 [T., Hillamo, R., Allan, J., Mentel, T. F., Tiitta, P., Laaksonen, A., Petäjä, T., Kulmala, M., Worsnop, D. R. and](#)  
770 [Facchini, M. C.: Determination of the biogenic secondary organic aerosol fraction in the boreal forest by NMR](#)  
771 [spectroscopy. \*Atmos. Chem. Phys.\*, 12\(2\), 941–959, doi:10.5194/acp-12-941-2012, 2012.](#)

772 [Ford, B., Val Martin, M., Zelasky, S. E., Fischer, E. V., Anenberg, S. C., Heald, C. L. and Pierce, J. R.: Future Fire](#)  
773 [Impacts on Smoke Concentrations, Visibility, and Health in the Contiguous United States, \*GeoHealth\*, 2\(8\), 229–](#)  
774 [247, doi:10.1029/2018gh000144, 2018.](#)

775 [Forrister, Haviland; Liu, Jiumeng; Scheuer, Eric; Dibb, Jack; Ziemba, Luke; Thornhill, L. Kenneth; Anderson, Bruce;](#)  
776 [Diskin, Glenn; Perring, E. Anne; P. Schwarz, Joshua; Campuzano-Jost, Pedro; A. Day, Douglas; B. Palm, Brett;](#)  
777 [Jimenez, L. Jose; Nenes, Athan, R. J.: Evolution of brown carbon in wildfire plumes. \*Geophys. Res. Lett.\*, 42,](#)  
778 [4623–4630, doi:10.1002/2015GL063897, 2015.](#)

779 [Foster, K., Pokhrel, R., Burkhart, M. and Murphy, S.: A novel approach to calibrating a photoacoustic absorption](#)  
780 [spectrometer using polydisperse absorbing aerosol, \*Atmos. Meas. Tech.\*, 12\(6\), 3351–3363, doi:10.5194/amt-12-](#)  
781 [3351-2019, 2019.](#)

782 [Fuller, K. A. and Kreidenweis, S. M.: Effects of mixing on extinction by carbonaceous particles, \*J. Geophys. Res.\*,](#)  
783 [104\(D13\), 15941–15954, doi:10.1029/1998JD100069, 1999.](#)

784 [Garofalo, L. A., Pothier, M. A., Levin, E. J. T., Campos, T., Kreidenweis, S. M. and Farmer, D. K.: Emission and](#)  
785 [Evolution of Submicron Organic Aerosol in Smoke from Wildfires in the Western United States. \*ACS Earth Sp.\*](#)  
786 [Chem., 3\(7\), 1237–1247, doi:10.1021/acsearthspacechem.9b00125, 2019.](#)

787 [Gouw, J. A. De, Middlebrook, A. M., Warneke, C., Goldan, P. D., Kuster, W. C., Roberts, J. M., Fehsenfeld, F. C.,](#)  
788 [Worsnop, D. R., Canagaratna, M. R., Pszenny, A. A. P., Keene, W. C., Marchewka, M., Bertman, S. B. and Bates,](#)  
789 [T. S.: Budget of organic carbon in a polluted atmosphere : Results from the New England Air Quality Study in](#)  
790 [2002. \*J. Geophys. Res.\*, 110, 1–22, doi:10.1029/2004JD005623, 2005.](#)

791 [Grieshop, A. P., Logue, J. M., Donahue, N. M. and Robinson, A. L.: Laboratory investigation of photochemical](#)  
792 [oxidation of organic aerosol from wood fires 1: Measurement and simulation of organic aerosol evolution, \*Atmos.\*](#)  
793 [Chem. Phys., 9\(4\), 1263–1277, doi:10.5194/acp-9-1263-2009, 2009.](#)

794 [Healy, R. M., Wang, J. M., Jeong, C. H., Lee, A. K. Y., Willis, M. D., Jaroudi, E., Zimmerman, N., Hilker, N., Murphy,](#)  
795 [M., Eckhardt, S., Stohl, A., Abbatt, J. P. D., Wenger, J. C. and Evans, G. J.: Light-absorbing properties of ambient](#)  
796 [black carbon and brown carbon from fossil fuel and biomass burning sources, \*J. Geophys. Res. Atmos.\*, 120\(13\),](#)  
797 [6619–6633, doi:10.1002/2015JD023382, 2015.](#)

798 [Hecobian, A., Zhang, X., Zheng, M., Frank, N., Edgerton, E. S. and Weber, R. J.: Water-soluble organic aerosol](#)  
799 [material and the light-absorption characteristics of aqueous extracts measured over the Southeastern United States,](#)  
800 [Atmos. Chem. Phys., 10\(13\), 5965–5977, doi:10.5194/acp-10-5965-2010, 2010.](#)

801 [Hurteau, M. D., Westerling, A. L., Wiedinmyer, C. and Bryant, B. P.: Projected effects of climate and development on](#)  
802 [California wildfire emissions through 2100, \*Environ. Sci. Technol.\*, 48\(4\), 2298–2304, doi:10.1021/es4050133,](#)  
803 [2014.](#)

804 [Kelesidis, G. A., Neubauer, D., Fan, L. S., Lohmann, U. and Pratsinis, S. E.: Enhanced Light Absorption and Radiative](#)  
805 [Forcing by Black Carbon Agglomerates, \*Environ. Sci. Technol.\*, 56\(12\), 8610–8618, doi:10.1021/acs.est.2c00428,](#)  
806 [2022.](#)

807 [Kirchstetter, T. W., Novakov, T. and Hobbs, P. V.: Evidence that the spectral dependence of light absorption by aerosols](#)  
808 [is affected by organic carbon, \*J. Geophys. Res. D Atmos.\*, 109\(21\), 1–12, doi:10.1029/2004JD004999, 2004.](#)

809 [Krasowsky, T. S., McMeeking, G. R., Wang, D., Sioutas, C. and Ban-Weiss, G. A.: Measurements of the impact of](#)  
810 [atmospheric aging on physical and optical properties of ambient black carbon particles in Los Angeles, \*Atmos.\*](#)  
811 [Environ., 142, 496–504, doi:10.1016/j.atmosenv.2016.08.010, 2016.](#)

812 [Lack, D. A., Lovejoy, E. R., Baynard, T., Pettersson, A. and Ravishankara, A. R.: Aerosol Absorption Measurement](#)  
813 [using Photoacoustic Spectroscopy: Sensitivity, Calibration, and Uncertainty Developments, \*Aerosol Sci. Technol.\*,](#)  
814 [40\(9\), 697–708, doi:10.1080/02786820600803917, 2006.](#)

815 [Lack, D. A. and Cappa, C. D.: Impact of brown and clear carbon on light absorption enhancement, single scatter](#)  
816 [albedo and absorption wavelength dependence of black carbon, \*Atmos. Chem. Phys.\*, 10\(9\), 4207–4220,](#)  
817 [doi:10.5194/acp-10-4207-2010, 2010.](#)

818 [Lack, D. A., Langridge, J. M., Bahreini, R., Cappa, C. D., Middlebrook, A. M. and Schwarz, J. P.: Brown carbon and](#)  
819 [internal mixing in biomass burning particles, \*Proc. Natl. Acad. Sci. U. S. A.\*, 109\(37\), 14802–14807,](#)  
820 [doi:10.1073/pnas.1206575109, 2012a.](#)

821 [Lack, D. A., Richardson, M. S., Law, D., Langridge, J. M., Cappa, C. D., McLaughlin, R. J. and Murphy, D. M.:](#)  
822 [Aircraft Instrument for Comprehensive Characterization of Aerosol Optical Properties, Part 2: Black and Brown](#)  
823 [Carbon Absorption and Absorption Enhancement Measured with Photo Acoustic Spectroscopy, \*Aerosol Sci.\*](#)  
824 [Technol., 46\(5\), 555–568, doi:10.1080/02786826.2011.645955, 2012b.](#)

825 [Lindaas, J., Pollack, I. B., Garofalo, L. A., Pothier, M. A., Farmer, D. K., Kreidenweis, S. M., Campos, T. L., Flocke,](#)  
826 [F., Weinheimer, A. J., Montzka, D. D., Tyndall, G. S., Palm, B. B., Peng, Q., Thornton, J. A., Permar, W., Wielgasz,](#)  
827 [C., Hu, L., Ottmar, R. D., Restaino, J. C., Hudak, A. T., Ku, I. T., Zhou, Y., Sive, B. C., Sullivan, A., Collett, J. L.,](#)  
828 [and Fischer, E. V.: Emissions of Reactive Nitrogen From Western U.S. Wildfires During Summer 2018, \*J. Geophys.\*](#)  
829 [Res. Atmos., 126\(2\), 1–21, doi:10.1029/2020JD032657, 2021.](#)

830 [Liu, D., Whitehead, J., Alfara, M. R., Reyes-villegas, E., Spracklen, D. V., Reddington, C. L., Kong, S., Williams, P.](#)  
831 [L., Ting, Y., Haslett, S., Taylor, J. W., Flynn, M. J., Morgan, W. T., Mcfiggans, G., Coe, H. and Allan, J. D.: Black-](#)  
832 [carbon absorption enhancement in the atmosphere determined by particle mixing state, \*Nat. Geosci.\*, 10\(3\), 184–](#)  
833 [188, doi:10.1038/NGEO2901, 2017.](#)

834 [Liu, D., He, C., Schwarz, J. P. and Wang, X.: Lifecycle of light-absorbing carbonaceous aerosols in the atmosphere,](#)  
835 [npj Clim. Atmos. Sci., 3\(40\), doi:10.1038/s41612-020-00145-8, 2020.](#)

836 [Liu, J., Bergin, M., Guo, H., King, L., Kotra, N., Edgerton, E. and Weber, R. J.: Size-resolved measurements of brown](#)  
837 [carbon in water and methanol extracts and estimates of their contribution to ambient fine-particle light absorption,](#)  
838 [Atmos. Chem. Phys., 13\(24\), 12389–12404, doi:10.5194/acp-13-12389-2013, 2013.](#)

839 [Liu, S., Aiken, A. C., Gorkowski, K., Dubey, M. K., Cappa, C. D., Williams, L. R., Herndon, S. C., Massoli, P., Fortner,](#)  
840 [E. C., Chhabra, P. S., Brooks, W. A., Onasch, T. B., Jayne, J. T., Worsnop, D. R., China, S., Sharma, N., Mazzoleni,](#)  
841 [C., Xu, L., Ng, N. L., Liu, D., Allan, J. D., Lee, J. D., Fleming, Z. L., Mohr, C., Zotter, P., Szidat, S. and Prévôt,](#)  
842 [A. S. H.: Enhanced light absorption by mixed source black and brown carbon particles in UK winter, Nat.](#)  
843 [Commun., 6, 8435, doi:10.1038/ncomms9435, 2015.](#)

844 [Marple, V. A., Rubow, K. L. and Behm, S. M.: A microorifice uniform deposit impactor \(moudi\): Description,](#)  
845 [calibration, and use, Aerosol Sci. Technol., 14\(4\), 434–436, doi:10.1080/02786829108959504, 1991.](#)

846 [McClure, C. D., Lim, C. Y., Hagan, D. H., Kroll, J. H. and Cappa, C. D.: Biomass-burning-derived particles from a](#)  
847 [wide variety of fuels - Part 1: Properties of primary particles, Atmos. Chem. Phys., 20\(3\), 1531–1547,](#)  
848 [doi:10.5194/acp-20-1531-2020, 2020.](#)

849 [McConnell, J. R., Edwards, R., Kok, L. G., Flanner, M. G., Zender, C. S., Saltzman, E. S., Banta, J. R., Pasteris, D.,](#)  
850 [R., Carter, M. M. and Kahl, J. D. W.: 20th-Century Industrial Black Carbon Emissions Altered Arctic Climate](#)  
851 [Forcing, Science \(80-. \), 317\(5843\), 1381–1384, doi:10.1126/science.1144856, 2007.](#)

852 [Moharreri, A., Craig, L., Dubey, P., Rogers, D. C. and Dhaniyala, S.: Aircraft testing of the new Blunt-body Aerosol](#)  
853 [Sampler \(BASE\), Atmos. Meas. Tech., 7\(9\), 3085–3093, doi:10.5194/amt-7-3085-2014, 2014.](#)

854 [Neumann, J. E., Amend, M., Anenberg, S., Kinney, P. L., Sarofim, M., Martinich, J., Lukens, J., Xu, J. W. and Roman,](#)  
855 [H.: Estimating PM2.5-related premature mortality and morbidity associated with future wildfire emissions in the](#)  
856 [western US, Environ. Res. Lett., 16\(3\), doi:10.1088/1748-9326/abe82b, 2021.](#)

857 [Onasch, T. B., Massoli, P., Keibian, P. L., Hills, F. B., Bacon, F. W. and Freedman, A.: Single scattering albedo](#)  
858 [monitor for airborne particulates, Aerosol Sci. Technol., 49\(4\), 267–279, doi:10.1080/02786826.2015.1022248,](#)  
859 [2015.](#)

860 [Orsini, D. A., Ma, Y., Sullivan, A., Sierau, B., Baumann, K. and Weber, R. J.: Refinements to the particle-into-liquid](#)  
861 [sampler \(PILS\) for ground and airborne measurements of water soluble aerosol composition, Atmos. Environ.,](#)  
862 [37\(9–10\), 1243–1259, doi:10.1016/S1352-2310\(02\)01015-4, 2003.](#)

863 [Palm, B. B., Peng, Q., Fredrickson, C. D., Lee, B. H., Garofalo, L. A., Pothier, M. A., Kreidenweis, S. M., Farmer, D.](#)  
864 [K., Pokhrel, R. P., Shen, Y., Murphy, S. M., Permar, W., Hu, L., Campos, T. L., Hall, S. R., Ullmann, K., Zhang,](#)  
865 [X., Flocke, F., Fischer, E. V. and Thornton, J. A.: Quantification of organic aerosol and brown carbon evolution in](#)  
866 [fresh wildfire plumes, Proc. Natl. Acad. Sci. U. S. A., 117\(47\), 29469–29477, doi:10.1073/pnas.2012218117, 2020.](#)

867 [Peltier, R. E., Weber, R. J. and Sullivan, A. P.: Investigating a liquid-based method for online organic carbon detection](#)  
868 [in atmospheric particles, Aerosol Sci. Technol., 41\(12\), 1117–1127, doi:10.1080/02786820701777465, 2007.](#)

869 [Peng, J., Hu, M., Guo, S., Du, Z., Zheng, J., Shang, D., Zamora, M. L., Zeng, L., Shao, M., Wu, Y. S., Zheng, J., Wang,](#)  
870 [Y., Glen, C. R., Collins, D. R., Molina, M. J. and Zhang, R.: Markedly enhanced absorption and direct radiative](#)  
871 [forcing of black carbon under polluted urban environments, Proc. Natl. Acad. Sci. U. S. A., 113\(16\), 4266–4271,](#)  
872 [doi:10.1073/pnas.1602310113, 2016.](#)



873 [Permar, W., Wang, Q., Selimovic, V., Wielgasz, C., Yokelson, R. J., Hornbrook, R. S., Hills, A. J., Apel, E. C., Ku, I.](#)  
874 [T., Zhou, Y., Sive, B. C., Sullivan, A. P., Collett, J. L., Campos, T. L., Palm, B. B., Peng, Q., Thornton, J. A.,](#)  
875 [Garofalo, L. A., Farmer, D. K., Kreidenweis, S. M., Levin, E. J. T., DeMott, P. J., Flocke, F., Fischer, E. V. and Hu,](#)  
876 [L.: Emissions of Trace Organic Gases From Western U.S. Wildfires Based on WE-CAN Aircraft Measurements,](#)  
877 [J. Geophys. Res. Atmos., 126\(11\), doi:10.1029/2020JD033838, 2021.](#)

878 [Pokhrel, R. P., Wagner, N. L., Langridge, J. M., Lack, D. A., Jayarathne, T., Stone, E. A., Stockwell, C. E., Yokelson,](#)  
879 [R. J. and Murphy, S. M.: Parameterization of single-scattering albedo \(SSA\) and absorption Ångström exponent](#)  
880 [\(AAE\) with EC/OC for aerosol emissions from biomass burning, Atmos. Chem. Phys., 16\(15\), 9549–9561,](#)  
881 [doi:10.5194/acp-16-9549-2016, 2016.](#)

882 [Pokhrel, R. P., Beamesderfer, E. R., Wagner, N. L., Langridge, J. M., Lack, D. A., Jayarathne, T., Stone, E. A.,](#)  
883 [Stockwell, C. E., Yokelson, R. J. and Murphy, S. M.: Relative importance of black carbon, brown carbon, and](#)  
884 [absorption enhancement from clear coatings in biomass burning emissions, Atmos. Chem. Phys., 17\(8\), 5063–](#)  
885 [5078, doi:10.5194/acp-17-5063-2017, 2017.](#)

886 [Romshoo, B., Müller, T., Pfeifer, S., Saturno, J., Nowak, A., Ciupek, K., Quincey, P. and Wiedensohler, A.: Optical](#)  
887 [properties of coated black carbon aggregates: Numerical simulations, radiative forcing estimates, and size-resolved](#)  
888 [parameterization scheme, Atmos. Chem. Phys., 21\(17\), 12989–13010, doi:10.5194/acp-21-12989-2021, 2021.](#)

889 [Rosencwaig, A.: Photoacoustic spectroscopy., Annu. Rev. Biophys. Bioeng., 9, 31–54,](#)  
890 [doi:10.1146/annurev.bb.09.060180.000335, 1980.](#)

891 [Saleh, R., Robinson, E. S., Tkacik, D. S., Ahern, A. T., Liu, S., Aiken, A. C., Sullivan, R. C., Presto, A. A., Dubey, M.](#)  
892 [K., Yokelson, R. J., Donahue, N. M. and Robinson, A. L.: Brownness of organics in aerosols from biomass burning](#)  
893 [linked to their black carbon content, Nat. Geosci., 7\(9\), 647–650, doi:10.1038/ngeo2220, 2014.](#)

894 [Saleh, R.: From Measurements to Models: Toward Accurate Representation of Brown Carbon in Climate Calculations,](#)  
895 [Curr. Pollut. Reports, 6\(2\), 90–104, doi:10.1007/s40726-020-00139-3, 2020.](#)

896 [Sarangi, C., Qian, Y., Rittger, K., Leung, R. L., Chand, D., Bormann, K. J. and Painter, T. H.: Dust dominates high-](#)  
897 [altitude snow darkening and melt over high-mountain Asia, Nat. Clim. Chang., \(October\), 1–7,](#)  
898 [doi:10.1038/s41558-020-00909-3, 2020.](#)

899 [Schnaiter, M., Horvath, H., Möhler, O., Naumann, K. H., Saathoff, H. and Schöck, O. W.: UV-VIS-NIR spectral optical](#)  
900 [properties of soot and soot-containing aerosols, J. Aerosol Sci., 34\(10\), 1421–1444, doi:10.1016/S0021-](#)  
901 [8502\(03\)00361-6, 2003.](#)

902 [Schnaiter, M., Linke, C., Möhler, O., Naumann, K. H., Saathoff, H., Wagner, R., Schurath, U. and Wehner, B.:](#)  
903 [Absorption amplification of black carbon internally mixed with secondary organic aerosol, J. Geophys. Res. D](#)  
904 [Atmos., 110\(19\), 1–11, doi:10.1029/2005JD006046, 2005.](#)

905 [Schwarz, J. P., Gao, R. S., Fahey, D. W., Thomson, D. S., Watts, L. A., Wilson, J. C., Reeves, J. M., Darbeheshti, M.,](#)  
906 [Baumgardner, D. G., Kok, G. L., Chung, S. H., Schulz, M., Hendricks, J., Lauer, A., Ka, B., Slowik, J. G., Rosenlof,](#)  
907 [K. H., Thompson, T. L., Langford, A. O., Loewenstein, M. and Aikin, K. C.: Single-particle measurements of](#)  
908 [midlatitude black carbon and light-scattering aerosols from the boundary layer to the lower stratosphere, J.](#)  
909 [Geophys. Res., 111, D16207, doi:10.1029/2006JD007076, 2006.](#)

910 [Subramanian, R., Kok, G. L., Baumgardner, D., Clarke, A., Shinozuka, Y., Campos, T. L., Heizer, C. G., Stephens, B.](#)  
911 [B., De Foy, B., Voss, P. B. and Zaveri, R. A.: Black carbon over Mexico: The effect of atmospheric transport on](#)  
912 [mixing state, mass absorption cross-section, and BC/CO ratios, \*Atmos. Chem. Phys.\*, 10\(1\), 219–237,](#)  
913 [doi:10.5194/acp-10-219-2010, 2010.](#)

914 [Sullivan, A. P., Pokhrel, R. P., Shen, Y., Murphy, S. M., Toohey, D. W., Campos, T., Lindaas, J., Fischer, E. V. and](#)  
915 [Collett, J. L.: Examination of Brown Carbon Absorption from Wildfires in the Western U.S. During the WE-CAN](#)  
916 [Study, \*Atmos. Chem. Phys. Discuss.\*, \(July\), 1–29, doi:10.5194/acp-2022-459, 2022.](#)

917 [Sun, Y., Zhang, Q., Zheng, M., Ding, X., Edgerton, E. S. and Wang, X.: Characterization and source apportionment](#)  
918 [of water-soluble organic matter in atmospheric fine particles \(PM<sub>2.5</sub>\) with high-resolution aerosol mass](#)  
919 [spectrometry and GC-MS, \*Environ. Sci. Technol.\*, 45\(11\), 4854–4861, doi:10.1021/es200162h, 2011.](#)

920 [Szopa, S., V. Naik, B. Adhikary, P. Artaxo, T. Berntsen, W.D. Collins, S. Fuzzi, L. Gallardo, A. Kiendler-Scharr, Z.](#)  
921 [Klimont, H. Liao, N. Unger, and P. Zanis: Short-Lived Climate Forcers. In \*Climate Change 2021: The Physical\*](#)  
922 [Science Basis. Contribution of Working Group I to the Sixth Assessment Report of the Intergovernmental Panel](#)  
923 [on Climate Change. Cambridge University Press, Cambridge, United Kingdom and New York, NY, USA, pp. 817–](#)  
924 [922, doi:10.1017/9781009157896.008, 2021.](#)

925 [Tasoglou, A., Louvaris, E., Florou, K., Liangou, A., Karnezi, E., Kaltsonoudis, C., Wang, N. and Pandis, S. N.: Aerosol](#)  
926 [light absorption and the role of extremely low volatility organic compounds, \*Atmos. Chem. Phys.\*, 20\(19\), 11625–](#)  
927 [11637, doi:10.5194/acp-20-11625-2020, 2020.](#)

928 [Taylor, J. W., Wu, H., Szpek, K., Bower, K., Crawford, I., Flynn, M. J., Williams, P. I., Dorsey, J., Langridge, J. M.,](#)  
929 [Cotterell, M. I., Fox, C., Davies, N. W., Haywood, J. M. and Coe, H.: Absorption closure in highly aged biomass](#)  
930 [burning smoke, \*Atmos. Chem. Phys.\*, 20\(19\), 11201–11221, doi:10.5194/acp-20-11201-2020, 2020.](#)

931 [Wang, X., Sedlacek, A. J., DeSá, S. S., Martin, S. T., Alexander, M. L., Alexander, M. L., Watson, T. B., Aiken, A. C.,](#)  
932 [Springston, S. R. and Artaxo, P.: Deriving brown carbon from multiwavelength absorption measurements: Method](#)  
933 [and application to AERONET and Aethalometer observations, \*Atmos. Chem. Phys.\*, 16\(19\), 12733–12752,](#)  
934 [doi:10.5194/acp-16-12733-2016, 2016.](#)

935 [Wang, X., Heald, C. L., Liu, J., Weber, R. J., Campuzano-Jost, P., Jimenez, J. L., Schwarz, J. P. and Perring, A. E.:](#)  
936 [Exploring the observational constraints on the simulation of brown carbon, \*Atmos. Chem. Phys.\*, 18\(2\), 635–653,](#)  
937 [doi:10.5194/acp-18-635-2018, 2018.](#)

938 [Wei, Y., Ma, L., Cao, T., Zhang, Q., Wu, J., Buseck, P. R. and Thompson, J. E.: Light scattering and extinction](#)  
939 [measurements combined with laser-induced incandescence for the real-time determination of soot mass absorption](#)  
940 [cross section, \*Anal. Chem.\*, 85\(19\), 9181–9188, doi:10.1021/ac401901b, 2013.](#)

941 [Westerling, A. L., Hidalgo, H. G., Cayan, D. R. and Swetnam, T. W.: Warming and Earlier Spring Increase Western](#)  
942 [U. S. Forest Wildfire Activity, \*Science\*, 313\(5789\), 940–943, doi:10.1126/science.1128834, 2006.](#)

943 [Williams, E. L. and Grosjean, D.: Removal of Atmospheric Oxidants with Annular Denuders, \*Environ. Sci. Technol.\*,](#)  
944 [24\(6\), 811–814, doi:10.1021/es00076a002, 1990.](#)

945 [Wonaschütz, A., Hitznerberger, R., Bauer, H., Pouresmaeil, P., Klatzer, B., Caseiro, A. and Puxbaum, H.: Application](#)  
946 [of the integrating sphere method to separate the contributions of brown and black carbon in atmospheric aerosols,](#)  
947 [Environ. Sci. Technol., 43\(4\), 1141–1146, doi:10.1021/es8008503, 2009.](#)

948 [Yue, X., Mickley, L. J., Logan, J. A. and Kaplan, J. O.: Ensemble projections of wildfire activity and carbonaceous](#)  
949 [aerosol concentrations over the western United States in the mid-21st century, Atmos. Environ., 77, 767–780,](#)  
950 [doi:10.1016/j.atmosenv.2013.06.003, 2013.](#)

951 [Zeng, L., Zhang, A., Wang, Y., Wagner, N. L., Katich, J. M., Schwarz, J. P., Schill, G. P., Brock, C., Froyd, K. D.,](#)  
952 [Murphy, D. M., Williamson, C. J., Kupc, A., Scheuer, E., Dibb, J. and Weber, R. J.: Global Measurements of Brown](#)  
953 [Carbon and Estimated Direct Radiative Effects, Geophys. Res. Lett., 47\(13\), doi:10.1029/2020GL088747, 2020.](#)

954 [Zeng, L., Sullivan, A. P., Washenfelder, R. A., Dibb, J., Scheuer, E., Campos, T. L., Katich, J. M., Levin, E., Robinson,](#)  
955 [M. A. and Weber, R. J.: Assessment of online water-soluble brown carbon measuring systems for aircraft sampling,](#)  
956 [Atmos. Meas. Tech., 14\(10\), 6357–6378, doi:10.5194/amt-14-6357-2021, 2021.](#)

957 [Zeng, L., Dibb, J., Scheuer, E., Katich, J. M., Schwarz, J. P., Bourgeois, I., Peischl, J., Ryerson, T., Warneke, C.,](#)  
958 [Perring, A. E., Diskin, G. S., Digangi, J. P., Nowak, J. B., Moore, R. H., Wiggins, E. B., Pagonis, D., Guo, H.,](#)  
959 [Campuzano-jost, P., Jimenez, J. L., Xu, L. and Weber, R. J.: Characteristics and Evolution of Brown Carbon in](#)  
960 [Western United States Wildfires, Atmos. Chem. Phys., 22, 8009–8036, doi:10.5194/acp-22-8009-2022, 2022.](#)

961 [Zhang, L., Segal-Rozenhaimer, M., Che, H., Dang, C., Sedlacek, A. J., Lewis, E. R., Dobracki, A., Wong, J. P. S.,](#)  
962 [Formenti, P., Howell, S. G. and Nenes, A.: Light absorption by brown carbon over the South-East Atlantic Ocean,](#)  
963 [Atmos. Chem. Phys., 22\(14\), 9199–9213, doi:10.5194/acp-22-9199-2022, 2022.](#)

964 [Zhang, Y., Forrister, H., Liu, J., Dibb, J., Anderson, B., Schwarz, J. P., Perring, A. E., Jimenez, J. L., Campuzano-Jost,](#)  
965 [P., Wang, Y., Nenes, A. and Weber, R. J.: Top-of-atmosphere radiative forcing affected by brown carbon in the](#)  
966 [upper troposphere, Nat. Geosci., 10\(7\), 486–489, doi:10.1038/ngeo2960, 2017.](#)

967 [Aiken, A. C., Decarlo, P. F., Kroll, J. H., Worsnop, D. R., Huffman, J. A., Docherty, K. S., et al. \(2008\). O/C and](#)  
968 [OM/OC ratios of primary, secondary, and ambient organic aerosols with high-resolution time-of-flight aerosol](#)  
969 [mass spectrometry. Environmental Science and Technology, 42\(12\), 4478–4485.](#)  
970 <https://doi.org/10.1021/es703009g>

971 [Akagi, S. K., Yokelson, R. J., Wiedinmyer, C., Alvarado, M. J., Reid, J. S., Karl, T., et al. \(2011\). Emission factors](#)  
972 [for open and domestic biomass burning for use in atmospheric models. Atmospheric Chemistry and Physics,](#)  
973 [11\(9\), 4039–4072. https://doi.org/10.5194/acp-11-4039-2011](#)

974 [Andreae, M. O. \(2019\). Emission of trace gases and aerosols from biomass burning—An updated assessment.](#)  
975 [Atmospheric Chemistry and Physics Discussions, 1–27. https://doi.org/10.5194/acp-2019-303](#)

976 [Andreae, M. O., & Gelencsér, A. \(2006\). Black carbon or brown carbon? The nature of light-absorbing carbonaceous](#)  
977 [aerosols. Atmospheric Chemistry and Physics, 6, 3131–3148. https://doi.org/10.5194/acp-6-3131-2006](#)

978 [Bahadur, R., Praveen, P. S., Xu, Y., & Ramanathan, V. \(2012\). Solar absorption by elemental and brown carbon](#)  
979 [determined from spectral observations. Proceedings of the National Academy of Sciences, 109\(43\), 17366–](#)  
980 [17371. https://doi.org/10.1073/pnas.1205910109](#)

981 Bohren, C. F., and Huffman, D. R. (1983). Absorption and Scattering of Light by Small Particles. John Wiley & Sons,  
982 Inc.

983 Bond, T. C., & Bergstrom, R. W. (2006). Light absorption by carbonaceous particles: An investigative review. *Aerosol*  
984 *Science and Technology*, 40(1), 27–67. <https://doi.org/10.1080/02786820500421521>

985 Bond, T. C., Habib, G., & Bergstrom, R. W. (2006). Limitations in the enhancement of visible light absorption due to  
986 mixing state. *Journal of Geophysical Research Atmospheres*, 111(20), 1–13.  
987 <https://doi.org/10.1029/2006JD007315>

988 Bond, T. C., Doherty, S. J., Fahey, D. W., Forster, P. M., Berntsen, T., Deangelo, B. J., et al. (2013). Bounding the  
989 role of black carbon in the climate system: A scientific assessment. *Journal of Geophysical Research*  
990 *Atmospheres*, 118(11), 5380–5552. <https://doi.org/10.1002/jgrd.50171>

991 Brown, H., Liu, X., Feng, Y., Jiang, Y., Wu, M., Lu, Z., et al. (2018). Radiative effect and climate impacts of brown  
992 carbon with the Community Atmosphere Model (CAM5). *Atmospheric Chemistry and Physics*, 18(24), 17745–  
993 17768. <https://doi.org/10.5194/acp-18-17745-2018>

994 Brown, H., Liu, X., Pokhrel, R., Murphy, S., Lu, Z., Saleh, R., et al. (2021). Biomass burning aerosols in most climate  
995 models are too absorbing. *Nature Communications*, 12(1), 1–15. <https://doi.org/10.1038/s41467-020-20482-9>

996 Burke, M., Driscoll, A., Heft Neal, S., Xue, J., Burney, J., & Wara, M. (2021). The changing risk and burden of  
997 wildfire in the United States. *Proceedings of the National Academy of Sciences of the United States of America*,  
998 118(2), 1–6. <https://doi.org/10.1073/PNAS.2011048118>

999 Canagaratna, M. R., Jimenez, J. L., Kroll, J. H., Chen, Q., Kessler, S. H., Massoli, P., et al. (2015). Elemental ratio  
1000 measurements of organic compounds using aerosol mass spectrometry: characterization, improved calibration,  
1001 and implications. *Atmospheric Chemistry and Physics*, 15(1), 253–272. <https://doi.org/10.5194/acp-15-253-2015>

1002

1003 Cappa, C. D., Onasch, T. B., Massoli, P., Worsnop, D. R., Bates, T. S., Cross, E. S., et al. (2012). Radiative absorption  
1004 enhancements due to the mixing state of atmospheric black carbon. *Science*, 337(6098), 1078–1081.  
1005 <https://doi.org/10.1126/science.1223447>

1006 Cappa, C. D., Zhang, X., Russell, L. M., Collier, S., Lee, A. K. Y., Chen, C. L., et al. (2019). Light Absorption by  
1007 Ambient Black and Brown Carbon and its Dependence on Black Carbon Coating State for Two California, USA,  
1008 Cities in Winter and Summer. *Journal of Geophysical Research: Atmospheres*, 124(3), 1550–1577.  
1009 <https://doi.org/10.1029/2018JD029501>

1010 Carter, T. S., Heald, C. L., Cappa, C. D., Kroll, J. H., Campos, T. L., Coe, H., et al. (2021). Investigating Carbonaceous  
1011 Aerosol and its Absorption Properties from Fires in the western US (WE-CAN) and southern Africa (ORACLES  
1012 and CLARIFY). *Journal of Geophysical Research Atmospheres*, 1–28. <https://doi.org/10.1029/2021JD034984>

1013 Chen, M., Sun, Z., Davis, J. M., Liu, Y. A., Corr, C. A., & Gao, W. (2019). Improving the mean and uncertainty of  
1014 ultraviolet multi filter rotating shadowband radiometer in situ calibration factors: Utilizing Gaussian process  
1015 regression with a new method to estimate dynamic input uncertainty. *Atmospheric Measurement Techniques*,  
1016 12(2), 935–953. <https://doi.org/10.5194/amt-12-935-2019>

- 017 Cho, C., Kim, S. W., Lee, M., Lim, S., Fang, W., Gustafsson, Ö., et al. (2019). Observation-based estimates of the  
018 mass absorption cross-section of black and brown carbon and their contribution to aerosol light absorption in  
019 East Asia. *Atmospheric Environment*, 212(November 2018), 65–74.  
020 <https://doi.org/10.1016/j.atmosenv.2019.05.024>
- 021 Craig, L., Moharreri, A., Schanot, A., Rogers, D. C., Dhaniyala, S., Craig, L., et al. (2013a). Characterizations of  
022 Cloud Droplet Shatter Artifacts in Two Airborne Aerosol Inlets. *Aerosol Science and Technology*, 47:6, 662–  
023 671. <https://doi.org/10.1080/02786826.2013.780648>
- 024 Craig, L., Schanot, A., Moharreri, A., Rogers, D. C., & Dhaniyala, S. (2013b). Design and Sampling Characteristics  
025 of a New Airborne Aerosol Inlet for Aerosol Measurements in Clouds. *Journal of Atmospheric and Oceanic*  
026 *Technology*, 30, 1123–1135. <https://doi.org/10.1175/JTECH-D-12-00168.1>
- 027 Craig, L., Moharreri, A., Rogers, D. C., Anderson, B., & Dhaniyala, S. (2014). Aircraft-Based Aerosol Sampling in  
028 Clouds: Performance Characterization of Flow-Restriction Aerosol Inlets. *Journal of Atmospheric and Oceanic*  
029 *Technology*, 31, 2512–2521. <https://doi.org/10.1175/JTECH-D-14-00022.1>
- 030 Duarte, R. M. B. O., Freire, S. M. S. C., & Duarte, A. C. (2015). Investigating the water-soluble organic functionality  
031 of urban aerosols using two-dimensional correlation of solid-state <sup>13</sup>C-NMR and FTIR spectral data.  
032 *Atmospheric Environment*, 116, 245–252. <https://doi.org/10.1016/j.atmosenv.2015.06.043>
- 033 Duarte, R. M. B. O., Piñeiro Iglesias, M., López-Mahía, P., Muniategui-Lorenzo, S., Moreda-Piñeiro, J., Silva, A. M.  
034 S., & Duarte, A. C. (2019). Comparative study of atmospheric water-soluble organic aerosols composition in  
035 contrasting suburban environments in the Iberian Peninsula Coast. *Science of the Total Environment*, 648, 430–  
036 441. <https://doi.org/10.1016/j.scitotenv.2018.08.171>
- 037 Eatough, D. J., Wadsworth, A., Eatough, D. A., Crawford, J. W., Hansen, L. D., & Lewis, E. A. (1993). A multiple-  
038 system, multi-channel diffusion denuder sampler for the determination of fine particulate organic material in  
039 the atmosphere. *Atmospheric Environment Part A, General Topics*, 27(8), 1213–1219.  
040 [https://doi.org/10.1016/0960-1686\(93\)90247-V](https://doi.org/10.1016/0960-1686(93)90247-V)
- 041 Finessi, E., Decesari, S., Paglione, M., Giulianelli, L., Carbone, C., Gilardoni, S., et al. (2012). Determination of the  
042 biogenic secondary organic aerosol fraction in the boreal forest by NMR spectroscopy. *Atmospheric Chemistry*  
043 *and Physics*, 12(2), 941–959. <https://doi.org/10.5194/acp-12-941-2012>
- 044 Ford, B., Val-Martin, M., Zelasky, S. E., Fischer, E. V., Anenberg, S. C., Heald, C. L., & Pierce, J. R. (2018). Future  
045 Fire Impacts on Smoke Concentrations, Visibility, and Health in the Contiguous United States. *GeoHealth*, 2(8),  
046 229–247. <https://doi.org/10.1029/2018gh000144>
- 047 Forrister, Haviland; Liu, Jiumeng; Scheuer, Eric; Dibb, Jack; Ziemba, Luke; Thornhill, L. Kenneth; Anderson, Bruce;  
048 Diskin, Glenn; Perring, E. Anne; P. Schwarz, Joshua; Campuzano-Jost, Pedro; A. Day, Douglas; B. Palm, Brett;  
049 Jimenez, L. Jose; Nenes, Athan, R. J. (2015). Evolution of brown carbon in wildfire plumes. *Geophysical*  
050 *Research Letters*, 42, 4623–4630. <https://doi.org/10.1002/2015GL063897>
- 051 Foster, K., Pokhrel, R., Burkhart, M., & Murphy, S. (2019). A novel approach to calibrating a photoacoustic absorption  
052 spectrometer using polydisperse absorbing aerosol. *Atmospheric Measurement Techniques*, 12(6), 3351–3363.  
053 <https://doi.org/10.5194/amt-12-3351-2019>

- 054 Fuller, K. A., & Kreidenweis, S. M. (1999). Effects of mixing on extinction by carbonaceous particles. *Journal of*  
055 *Geophysical Research*, 104(D13), 15941–15954. <https://doi.org/10.1029/1998JD100069>
- 056 Garofalo, L. A., Pothier, M. A., Levin, E. J. T., Campos, T., Kreidenweis, S. M., & Farmer, D. K. (2019). Emission  
057 and Evolution of Submicron Organic Aerosol in Smoke from Wildfires in the Western United States. *ACS Earth*  
058 *and Space Chemistry*, 3(7), 1237–1247. <https://doi.org/10.1021/acsearthspacechem.9b00125>
- 059 Grieshop, A. P., Logue, J. M., Donahue, N. M., & Robinson, A. L. (2009). Laboratory investigation of photochemical  
060 oxidation of organic aerosol from wood fires 1: Measurement and simulation of organic aerosol evolution.  
061 *Atmospheric Chemistry and Physics*, 9(4), 1263–1277. <https://doi.org/10.5194/acp-9-1263-2009>
- 062 Gouw, J. A. De, Middlebrook, A. M., Warneke, C., Goldan, P. D., Kuster, W. C., Roberts, J. M., et al. (2005). Budget  
063 of organic carbon in a polluted atmosphere: Results from the New England Air Quality Study in 2002. *Journal*  
064 *of Geophysical Research*, 110, 1–22. <https://doi.org/10.1029/2004JD005623>
- 065 Healy, R. M., Wang, J. M., Jeong, C. H., Lee, A. K. Y., Willis, M. D., Jaroudi, E., et al. (2015). Light-absorbing  
066 properties of ambient black carbon and brown carbon from fossil fuel and biomass-burning sources. *Journal of*  
067 *Geophysical Research: Atmospheres*, 120(13), 6619–6633. <https://doi.org/10.1002/2015JD023382>
- 068 Hecobian, A., Zhang, X., Zheng, M., Frank, N., Edgerton, E. S., & Weber, R. J. (2010). Water-soluble organic aerosol  
069 material and the light-absorption characteristics of aqueous extracts measured over the Southeastern United  
070 States. *Atmospheric Chemistry and Physics*, 10(13), 5965–5977. <https://doi.org/10.5194/acp-10-5965-2010>
- 071 Hurteau, M. D., Westerling, A. L., Wiedinmyer, C., & Bryant, B. P. (2014). Projected effects of climate and  
072 development on California wildfire emissions through 2100. *Environmental Science and Technology*, 48(4),  
073 2298–2304. <https://doi.org/10.1021/es4050133>
- 074 Kirchstetter, T. W., Novakov, T., & Hobbs, P. V. (2004). Evidence that the spectral dependence of light absorption  
075 by aerosols is affected by organic carbon. *Journal of Geophysical Research D: Atmospheres*, 109(21), 1–12.  
076 <https://doi.org/10.1029/2004JD004999>
- 077 Krasowsky, T. S., McMeeking, G. R., Wang, D., Sioutas, C., & Ban-Weiss, G. A. (2016). Measurements of the impact  
078 of atmospheric aging on physical and optical properties of ambient black carbon particles in Los Angeles.  
079 *Atmospheric Environment*, 142, 496–504. <https://doi.org/10.1016/j.atmosenv.2016.08.010>
- 080 Kleinman, L. I., Sedlacek, A. J., Adachi, K., Buseck, P. R., Collier, S., Dubey, M. K., et al. (2020). Rapid evolution  
081 of aerosol particles and their optical properties downwind of wildfires in the western US. *Atmospheric Chemistry*  
082 *and Physics*, 20(21), 13319–13341. <https://doi.org/10.5194/acp-20-13319-2020>
- 083 Lack, D. A., Lovejoy, E. R., Baynard, T., Pettersson, A., & Ravishankara, A. R. (2006). Aerosol Absorption  
084 Measurement using Photoacoustic Spectroscopy: Sensitivity, Calibration, and Uncertainty Developments.  
085 *Aerosol Science and Technology*, 40(9), 697–708. <https://doi.org/10.1080/02786820600803917>
- 086 Lack, D. A., & Cappa, C. D. (2010). Impact of brown and clear carbon on light absorption enhancement, single scatter  
087 albedo and absorption wavelength dependence of black carbon. *Atmospheric Chemistry and Physics*, 10(9),  
088 4207–4220. <https://doi.org/10.5194/acp-10-4207-2010>

- 089 Lack, D. A., Langridge, J. M., Bahreini, R., Cappa, C. D., Middlebrook, A. M., & Schwarz, J. P. (2012a). Brown  
 090 carbon and internal mixing in biomass-burning particles. *Proceedings of the National Academy of Sciences of*  
 091 *the United States of America*, *109*(37), 14802–14807. <https://doi.org/10.1073/pnas.1206575109>
- 092 Lack, D. A., Richardson, M. S., Law, D., Langridge, J. M., Cappa, C. D., McLaughlin, R. J., & Murphy, D. M. (2012b).  
 093 Aircraft Instrument for Comprehensive Characterization of Aerosol Optical Properties, Part 2: Black and Brown  
 094 Carbon Absorption and Absorption Enhancement Measured with Photo Acoustic Spectroscopy. *Aerosol Science*  
 095 *and Technology*, *46*(5), 555–568. <https://doi.org/10.1080/02786826.2011.645955>
- 096 Lindaas, J., Pollack, I. B., Garofalo, L. A., Pothier, M. A., Farmer, D. K., Kreidenweis, S. M., et al. (2021). Emissions  
 097 of Reactive Nitrogen From Western U.S. Wildfires During Summer 2018. *Journal of Geophysical Research:*  
 098 *Atmospheres*, *126*(2), 1–21. <https://doi.org/10.1029/2020JD032657>
- 099 Liu, D., Whitehead, J., Alfara, M. R., Reyes-villegas, E., Spracklen, D. V., Reddington, C. L., et al. (2017). Black-  
 100 carbon absorption enhancement in the atmosphere determined by particle mixing state. *Nature Geoscience*,  
 101 *10*(3), 184–188. <https://doi.org/10.1038/NGEO2901>
- 102 Liu, D., He, C., Schwarz, J. P., & Wang, X. (2020). Lifecycle of light-absorbing carbonaceous aerosols in the  
 103 atmosphere. *Npj Climate and Atmospheric Science*, *3*(40). <https://doi.org/10.1038/s41612-020-00145-8>
- 104 Liu, J., Bergin, M., Guo, H., King, L., Kotra, N., Edgerton, E., & Weber, R. J. (2013). Size-resolved measurements of  
 105 brown carbon in water and methanol extracts and estimates of their contribution to ambient fine particle light  
 106 absorption. *Atmospheric Chemistry and Physics*, *13*(24), 12389–12404. [https://doi.org/10.5194/acp-13-12389-](https://doi.org/10.5194/acp-13-12389-2013)  
 107 [2013](https://doi.org/10.5194/acp-13-12389-2013)
- 108 Liu, S., Aiken, A. C., Gorkowski, K., Dubey, M. K., Cappa, C. D., Williams, L. R., et al. (2015). Enhanced light  
 109 absorption by mixed-source black and brown carbon particles in UK winter. *Nature Communications*, *6*, 8435.  
 110 <https://doi.org/10.1038/ncomms9435>
- 111 Marple, V. A., Rubow, K. L., & Behm, S. M. (1991). A microorifice uniform deposit impactor (moudi): Description,  
 112 calibration, and use. *Aerosol Science and Technology*, *14*(4), 434–436.  
 113 <https://doi.org/10.1080/02786829108959504>
- 114 McClure, C. D., Lim, C. Y., Hagan, D. H., Kroll, J. H., & Cappa, C. D. (2020). Biomass-burning-derived particles  
 115 from a wide variety of fuels—Part 1: Properties of primary particles. *Atmospheric Chemistry and Physics*, *20*(3),  
 116 1531–1547. <https://doi.org/10.5194/acp-20-1531-2020>
- 117 McConnell, J. R., Edwards, R., Kok, L. G., Flanner, M. G., Zender, C. S., Saltzman, E. S., et al. (2007). 20th-Century  
 118 Industrial Black Carbon Emissions Altered Arctic Climate Forcing. *Science*, *317*(5843), 1381–1384.  
 119 <https://doi.org/10.1126/science.1144856>
- 120 Moharreri, A., Craig, L., Dubey, P., Rogers, D. C., & Dhaniyala, S. (2014). Aircraft testing of the new Blunt-body  
 121 Aerosol Sampler (BASE). *Atmospheric Measurement Techniques*, *7*(9), 3085–3093.  
 122 <https://doi.org/10.5194/amt-7-3085-2014>
- 123 Neumann, J. E., Amend, M., Anenberg, S., Kinney, P. L., Sarofim, M., Martinich, J., et al. (2021). Estimating PM<sub>2.5</sub>-  
 124 related premature mortality and morbidity associated with future wildfire emissions in the western US.  
 125 *Environmental Research Letters*, *16*(3). <https://doi.org/10.1088/1748-9326/abe82b>

126 Onasch, T. B., Massoli, P., Keibian, P. L., Hills, F. B., Bacon, F. W., & Freedman, A. (2015). Single-scattering  
127 albedo monitor for airborne particulates. *Aerosol Science and Technology*, 49(4), 267–279.  
128 <https://doi.org/10.1080/02786826.2015.1022248>

129 Orsini, D. A., Ma, Y., Sullivan, A., Sierau, B., Baumann, K., & Weber, R. J. (2003). Refinements to the particle into  
130 liquid sampler (PILS) for ground and airborne measurements of water soluble aerosol composition. *Atmospheric*  
131 *Environment*, 37(9–10), 1243–1259. [https://doi.org/10.1016/S1352-2310\(02\)01015-4](https://doi.org/10.1016/S1352-2310(02)01015-4)

132 Palm, B. B., Peng, Q., Fredrickson, C. D., Lee, B. H., Garofalo, L. A., Pothier, M. A., et al. (2020). Quantification of  
133 organic aerosol and brown carbon evolution in fresh wildfire plumes. *Proceedings of the National Academy of*  
134 *Sciences of the United States of America*, 117(47), 29469–29477. <https://doi.org/10.1073/pnas.2012218117>

135 Peltier, R. E., Weber, R. J., & Sullivan, A. P. (2007). Investigating a liquid-based method for online organic carbon  
136 detection in atmospheric particles. *Aerosol Science and Technology*, 41(12), 1117–1127.  
137 <https://doi.org/10.1080/02786820701777465>

138 Peng, J., Hu, M., Guo, S., Du, Z., Zheng, J., Shang, D., et al. (2016). Markedly enhanced absorption and direct radiative  
139 forcing of black carbon under polluted urban environments. *Proceedings of the National Academy of Sciences*  
140 *of the United States of America*, 113(16), 4266–4271. <https://doi.org/10.1073/pnas.1602310113>

141 Peng, Q., Palm, B. B., Melander, K. E., Lee, B. H., Hall, S. R., Ullmann, K., et al. (2020). HONO Emissions from  
142 Western U.S. Wildfires Provide Dominant Radical Source in Fresh Wildfire Smoke. *Environmental Science and*  
143 *Technology*, 54(10), 5954–5963. <https://doi.org/10.1021/acs.est.0c00126>

144 Permar, W., Wang, Q., Selimovic, V., Wielgasz, C., Yokelson, R. J., Hornbrook, R. S., et al. (2021). Emissions of  
145 Trace Organic Gases From Western U.S. Wildfires Based on WE-CAN Aircraft Measurements. *Journal of*  
146 *Geophysical Research: Atmospheres*, 126(11). <https://doi.org/10.1029/2020JD033838>

147 Pokhrel, R. P., Wagner, N. L., Langridge, J. M., Lack, D. A., Jayarathne, T., Stone, E. A., et al. (2016).  
148 Parameterization of single-scattering albedo (SSA) and absorption Ångström exponent (AAE) with EC/OC for  
149 aerosol emissions from biomass burning. *Atmospheric Chemistry and Physics*, 16(15), 9549–9561.  
150 <https://doi.org/10.5194/acp-16-9549-2016>

151 Pokhrel, R. P., Beamesderfer, E. R., Wagner, N. L., Langridge, J. M., Lack, D. A., Jayarathne, T., et al. (2017). Relative  
152 importance of black carbon, brown carbon, and absorption enhancement from clear coatings in biomass burning  
153 emissions. *Atmospheric Chemistry and Physics*, 17(8), 5063–5078. <https://doi.org/10.5194/acp-17-5063-2017>

154 Rosencwaig, A. (1980). *Photoacoustics and photoacoustic spectroscopy*. *Annual Review of Biophysics and*  
155 *Bioengineering*, 9, 31–54. <https://doi.org/10.1146/annurev.bb.09.060180.000335>

156 Saleh, R., Robinson, E. S., Tkacik, D. S., Ahern, A. T., Liu, S., Aiken, A. C., et al. (2014). Brownness of organics in  
157 aerosols from biomass burning linked to their black carbon content. *Nature Geoscience*, 7(9), 647–650.  
158 <https://doi.org/10.1038/ngeo2220>

159 Saleh, R. (2020). From Measurements to Models: Toward Accurate Representation of Brown Carbon in Climate  
160 Calculations. *Current Pollution Reports*, 6(2), 90–104. <https://doi.org/10.1007/s40726-020-00139-3>



- 161 Sarangi, C., Qian, Y., Rittger, K., Leung, R. L., Chand, D., Bormann, K. J., & Painter, T. H. (2020). Dust dominates  
162 high-altitude snow darkening and melt over high mountain Asia. *Nature Climate Change*, (October), 1–7.  
163 <https://doi.org/10.1038/s41558-020-00909-3>
- 164 Schnaiter, M., Horvath, H., Möhler, O., Naumann, K. H., Saathoff, H., & Schöck, O. W. (2003). UV–VIS–NIR spectral  
165 optical properties of soot and soot-containing aerosols. *Journal of Aerosol Science*, *34*(10), 1421–1444.  
166 [https://doi.org/10.1016/S0021-8502\(03\)00361-6](https://doi.org/10.1016/S0021-8502(03)00361-6)
- 167 Schnaiter, M., Linke, C., Möhler, O., Naumann, K. H., Saathoff, H., Wagner, R., et al. (2005). Absorption  
168 amplification of black carbon internally mixed with secondary organic aerosol. *Journal of Geophysical Research*  
169 *D: Atmospheres*, *110*(19), 1–11. <https://doi.org/10.1029/2005JD006046>
- 170 Schwarz, J. P., Gao, R. S., Fahey, D. W., Thomson, D. S., Watts, L. A., Wilson, J. C., et al. (2006). Single-particle  
171 measurements of midlatitude black carbon and light scattering aerosols from the boundary layer to the lower  
172 stratosphere. *Journal of Geophysical Research*, *111*, D16207. <https://doi.org/10.1029/2006JD007076>
- 173 Subramanian, R., Kok, G. L., Baumgardner, D., Clarke, A., Shinzuka, Y., Campos, T. L., et al. (2010). Black carbon  
174 over Mexico: The effect of atmospheric transport on mixing state, mass absorption cross-section, and BC/CO  
175 ratios. *Atmospheric Chemistry and Physics*, *10*(1), 219–237. <https://doi.org/10.5194/acp-10-219-2010>
- 176 Sullivan, A. P., Pokhrel, R. P., Shen, Y., Murphy, S. M., Toohey, D. W., Campos, T., Lindaas, J., Fischer, E. V., and  
177 Collett Jr., J. L. (2022). Examination of Brown Carbon Absorption from Wildfires in the Western U.S. During  
178 the WE-CAN Study. *Atmospheric Chemistry and Physics*, *22*(20), 13389–13406. <https://doi.org/10.5194/acp-22-13389-2022>
- 179
- 180 Sun, Y., Zhang, Q., Zheng, M., Ding, X., Edgerton, E. S., & Wang, X. (2011). Characterization and source  
181 apportionment of water-soluble organic matter in atmospheric fine particles (PM<sub>2.5</sub>) with high-resolution  
182 aerosol mass spectrometry and GC-MS. *Environmental Science and Technology*, *45*(11), 4854–4861.  
183 <https://doi.org/10.1021/es200162h>
- 184 Szopa, S., V. Naik, B. Adhikary, P. Artaxo, T. Berntsen, W.D. Collins, S. et al. (2021): Short-Lived Climate Forcers.  
185 In *Climate Change 2021: The Physical Science Basis. Contribution of Working Group I to the Sixth Assessment*  
186 *Report of the Intergovernmental Panel on Climate Change*. Cambridge University Press, Cambridge, United  
187 Kingdom and New York, NY, USA, pp. 817–922. <https://doi:10.1017/9781009157896.008>
- 188 Tasoglou, A., Louvaris, E., Florou, K., Liangou, A., Karnezi, E., Kaltsounoudis, C., et al. (2020). Aerosol light  
189 absorption and the role of extremely low volatility organic compounds. *Atmospheric Chemistry and Physics*,  
190 *20*(19), 11625–11637. <https://doi.org/10.5194/acp-20-11625-2020>
- 191 Taylor, J. W., Wu, H., Szpek, K., Bower, K., Crawford, I., Flynn, M. J., et al. (2020). Absorption closure in highly  
192 aged biomass burning smoke. *Atmospheric Chemistry and Physics*, *20*(19), 11201–11221.  
193 <https://doi.org/10.5194/acp-20-11201-2020>
- 194 Wang, X., Sedlacek, A. J., DeSá, S. S., Martin, S. T., Alexander, M. L., Alexander, M. L., et al. (2016). Deriving  
195 brown carbon from multiwavelength absorption measurements: Method and application to AERONET and  
196 Aethalometer observations. *Atmospheric Chemistry and Physics*, *16*(19), 12733–12752.  
197 <https://doi.org/10.5194/acp-16-12733-2016>

198 Wang, X., Heald, C. L., Liu, J., Weber, R. J., Campuzano Jost, P., Jimenez, J. L., et al. (2018). Exploring the  
199 observational constraints on the simulation of brown carbon. *Atmospheric Chemistry and Physics*, 18(2), 635–  
200 653. <https://doi.org/10.5194/aep-18-635-2018>

201 Wei, Y., Ma, L., Cao, T., Zhang, Q., Wu, J., Buseck, P. R., & Thompson, J. E. (2013). Light scattering and extinction  
202 measurements combined with laser-induced incandescence for the real-time determination of soot mass  
203 absorption cross section. *Analytical Chemistry*, 85(19), 9181–9188. <https://doi.org/10.1021/ac401901b>

204 Westerling, A. L., Hidalgo, H. G., Cayan, D. R., & Swetnam, T. W. (2006). Warming and Earlier Spring Increase  
205 Western U. S. Forest Wildfire Activity. *Science*, 313(5789), 940–943. <https://doi.org/10.1126/science.1128834>

206 Williams, E. L., & Grosjean, D. (1990). Removal of Atmospheric Oxidants with Annular Denuders. *Environmental  
207 Science and Technology*, 24(6), 811–814. <https://doi.org/10.1021/es00076a002>

208 Wonaschütz, A., Hitznerberger, R., Bauer, H., Pouresmaeil, P., Klatzer, B., Caseiro, A., & Puxbaum, H. (2009).  
209 Application of the integrating sphere method to separate the contributions of brown and black carbon in  
210 atmospheric aerosols. *Environmental Science and Technology*, 43(4), 1141–1146.  
211 <https://doi.org/10.1021/es8008503>

212 Yue, X., Mickley, L. J., Logan, J. A., & Kaplan, J. O. (2013). Ensemble projections of wildfire activity and  
213 carbonaceous aerosol concentrations over the western United States in the mid-21st century. *Atmospheric  
214 Environment*, 77, 767–780. <https://doi.org/10.1016/j.atmosenv.2013.06.003>

215 Zeng, L., Zhang, A., Wang, Y., Wagner, N. L., Katich, J. M., Schwarz, J. P., et al. (2020). Global Measurements of  
216 Brown Carbon and Estimated Direct Radiative Effects. *Geophysical Research Letters*, 47(13).  
217 <https://doi.org/10.1029/2020GL088747>

218 Zeng, L., Sullivan, A. P., Washenfelder, R. A., Dibb, J., Scheuer, E., Campos, T. L., et al. (2021). Assessment of  
219 online water-soluble brown carbon measuring systems for aircraft sampling. *Atmospheric Measurement  
220 Techniques*, 14(10), 6357–6378. <https://doi.org/10.5194/amt-14-6357-2021>

221 Zeng, L., Dibb, J., Scheuer, E., Katich, J. M., Schwarz, J. P., Bourgeois, I., et al. (2022). Characteristics and Evolution  
222 of Brown Carbon in Western United States Wildfires. *Atmospheric Chemistry and Physics*, 22, 8009–8036.  
223 <https://doi.org/10.5194/aep-22-8009-2022>

224 Zhang, L., Segal-Rozenhaimer, M., Che, H., Dang, C., Sedlacek III, A. J., Lewis, E. R., Dobracki, A., Wong, J. P. S.,  
225 Formenti, P., Howell, S. G., and Nenes, A.: Light Absorption by Brown Carbon over the South-East Atlantic  
226 Ocean, *Atmos. Chem. Phys. Discuss.* [preprint], <https://doi.org/10.5194/aep-2021-1000>, in review, 2022.

227 Zhang, Y., Forrister, H., Liu, J., Dibb, J., Anderson, B., Schwarz, J. P., et al. (2017). Top-of-atmosphere radiative  
228 forcing affected by brown carbon in the upper troposphere. *Nature Geoscience*, 10(7), 486–489.  
229 <https://doi.org/10.1038/ngeo2960>